CANCER

Cullin-5 deficiency orchestrates the tumor microenvironment to promote mammary tumor development through CREB1-CCL2 signaling

Si Chen[1,2], Fangyuan Shao[1,2], Jianming Zeng[1,2], Sen Guo[1,2], Lijian Wang[1,2], Heng Sun[1,2,3], Josh Haipeng Lei[1,2], Xueying Lyu[1,2], Shuai Gao[4], Qiang Chen[1,2,3], Kai Miao[1,2,3], Xiaoling Xu[1,2,3], Chu-Xia Deng[1,2,3]*

Breast cancer–associated gene 1 (*Brca1*) deficiency induces the onset of breast cancer formation, accompanied with extensive genetic alterations. Here, we used both the sleeping beauty transposon mutagenesis system and CRISPR-Cas9–mediated genome-wide screening in mice to identify potential genetic alterations that act synergistically with *Brca1* deficiency to promote tumorignesis. Both approaches identified Cullin-5 as a tumor suppressor, whose mutation enabled *Brca1*-deficient cell survival and accelerated tumorigenesis by orchestrating tumor microenvironment. Cullin-5 suppresses cell growth through ubiquitylating and degrading adenosine 3′,5′-monophosphate–responsive element binding protein 1 (CREB1), especially under protein damage condition. Meanwhile, Cullin-5 deficiency activated CREB1-CCL2 signaling and resulted in the accumulation of monocytes and polymorphonuclear myeloid–derived suppressor cells, reduction of T cells that benefit tumor progression in both *Brca1*-deficient cells and wild-type cells. Blocking CREB1 activity either through gene knockout or specific inhibitor treatment suppressed changes in the tumor microenvironment caused by Cullin-5 deficiency and blocked tumor progression.

INTRODUCTION

According to recent reports from the World Health Organization, approximately 2,260,000 new breast cancer cases (11.7% of all new cancer cases) had been diagnosed in 2020, claiming the lives of more than 684,990 patients (30.3% of new breast cancer cases), therefore making it the most common type of cancer. Thus, there is an urgent need to decrease the incidence of breast cancer and develop previously unidentified, more effective treatments.

Breast cancer is the accumulated consequence of malignant and intricate events caused by multiple genetic alterations (*1*). Dominant mutations cause the acquisition of hyperproliferation potential, disrupt normal biological processes, and initiate other genetic alterations to trigger tumorigenesis (*2*). Recent studies have identified some cancer driver genes, including *p53*, breast cancer–associated gene 1 (*Brca1*), *Brca2*, checkpoint kinase 2 (*Chk2*), and tumor protein p53 binding protein 1 (*53BP1*), and have demonstrated the involvement of these genes in carcinogenesis (*3*, *4*).

BRCA1 is a critical tumor suppressor in breast cancer and serves as the guardian to maintain genome stability through homologous recombination–mediated DNA double-strand break repair (*5*, *6*). *Brca1* mutation carriers have an age-dependent risk of developing breast cancer with a cumulative first breast cancer risk of 61.8% at or before 60 years of age (*7*) compared with 12.5% (or one in eight) in *Brca1* wild-type (WT) individuals. The absence of *Brca1* impairs DNA damage repair ability, thereby leading to DNA damage accumulation, which results in the inactivation of some tumor suppressors and activation of some oncogenes, ultimately promoting tumorigenesis (*8*, *9*). To determine the mechanisms underlying tumorigenesis associated with *Brca1* deficiency, we previously conducted mammary gland–specific disruption of *Brca1* in mice using an *MMTV-Cre*–mediated approach. Our results showed that approximately 25% of mutant mice ($Brca1^{Flox11/Flox11}$;*MMTV-Cre* mice) developed mammary tumors at an average age of 18 months (*10*), which was relatively late in the lifetime of mice. Loss of the tumor suppressor *p53* markedly accelerates tumorigenesis accompanied by massive genetic alterations (*11*), suggesting that some additional factors may be involved in tumor initiation and/or progression.

To identify the potential factors that may participate in *Brca1*-associated tumorigenesis, we had adapted a traditional genetic approach by interbreeding *Brca1*-mutant mice with mouse strains carrying targeted disruptions of *p53*, *p21*, *ATM*, *CHK2*, or *53BP1* genes (*4*, *12*–*14*). These studies not only demonstrated that loss of *p53* relaxes cell cycle control and attenuates apoptosis, which enables *Brca1*-deficient cells to survive and eventually become malignantly transformed, but also revealed the involvement of *ATM*, *p21*, *53BP1*, and *CHK2* in the *Brca1*-deficient background to trigger tumor formation (*4*, *13*). Because these studies could only test candidate genes one by one, we have also conducted an unbiased in vivo screening by integrating the sleeping beauty system (SB^{+};$T2Onc3^{+}$) (*15*) into the *Cre-LoxP*–mediated *Brca1* mammary gland–specific knockout (KO) ($Brca1^{Flox11/Flox11}$;*MMTV-Cre* and $Brca1^{Flox11/Flox11}$;*Wap-Cre*) mouse model. This study identified 169 candidate genes, among which *Notch1* was identified as a potent oncogene, whose activation enhances BRCA1-related tumorigenesis (*16*).

In the present study, we further analyzed this 169 gene list (*16*) and found that Cullin-5 (*Cul5*), which was ranked at the fourth

[1]Cancer Center, Faculty of Health Sciences, University of Macau, Macau SAR, China. [2]Institute of Translational Medicine, Faculty of Health Sciences, University of Macau, Macau SAR, China. [3]MOE Frontiers Science Center for Precision Oncogene, University of Macau, Macau SAR, China. [4]Key Laboratory of Animal Genetics, Breeding and Reproduction of the MARA, National Engineering Laboratory for Animal Breeding, College of Animal Science and Technology, China Agricultural University, Beijing, China.
*Corresponding author. Email: cxdeng@um.edu.mo

position in the list, acted as a top candidate tumor suppressor, whose disruption enhanced Brca1-related tumorigenesis. This notion was confirmed by our parallel whole-genome screening mediated by clustered regularly interspaced short palindromic repeats (CRISPR)–Cas9. Mechanistically, we found that CUL5 ubiquitylates adenosine 3′,5′-monophosphate (cAMP)–responsive binding protein 1 (CREB1) to degrade it under both regular and stress conditions to suppress tumorigenesis, and conversely, *Cul5* deficiency activated CREB1-CCL2, leading to tumor growth via induction of changes in the tumor microenvironment (TME).

RESULTS

Cul5 deficiency promotes BRCA1-associated tumorigenesis

Our analysis on 306 tumors developed in the *Brca1*$^{Flox11/Flox11}$*;MMTV-Cre;SB* mice and *Brca1*$^{Flox11/Flox11}$*;WAP-Cre;SB* mice (*16*) revealed that *Cul5* was mutated by Sleeping Beauty (SB) transposon insertion in 77 tumors developed in 65 mice. When comparing the tumor-free curves of *Brca1*-mutant mice with or without *Cul5*-SB insertion, we found that SB-mediated mutagenesis on *Cul5*-SB markedly enhanced the tumorigenesis (Fig. 1A). The insertion sites of the SB transposon spread across the entire *Cul5* locus with either in the same or against transcription direction at a random pattern (Fig. 1B), suggesting that the enhanced tumorigenesis was associated with loss-of-function mutations of *Cul5* in *Brca1*-deficient mice.

In parallel, for the purpose to identify more cancer drivers, we had also conducted genome-wide CRISPR-Cas9 library screenings in mouse embryonic fibroblasts (MEFs), which were freshly derived from 13.5-day *Brca1*$^{Flox11/Flox11}$*;mT/mG* embryos. The MEFs were infected with an adenovirus-expressing Cre to knock out *Brca1* exon 11, followed by fluorescence-activated cell sorting (FACS) to isolate the *Brca1*-mutant cells. Despite the slower growth of *Brca1*-mutant MEFs (*17*), we were about to obtain 1×10^7 mutant MEFs at one passage after sorting and immediately infected them with a lentivirus harboring a mouse GeCKOv2 single guide RNA (sgRNA) library (*18*) or control lentivirus, followed by continuous in vitro passaging under regular cell culture conditions (fig. S1A). Our data indicated that MEFs infected with the GeCKOv2 sgRNA library overcame the lethality caused by *Brca1* deficiency, whereas *Brca1*-mutant MEFs infected with control virus exhibited extremely poor growth rates and could not grow after passage 3 (Fig. 1C).

To identify the candidate genes whose alteration suppressed lethality caused by *Brca1* deficiency, we conducted next-generation sequencing (NGS) to identify sgRNAs in serial passages of MEFs and in tumors samples derived from nude mice with the implantation of MEF cells at passages 1 and 16 into their mammary fat pad (fig. S1B). While no tumors were formed in the recipient ($n = 6$) that received the injection of cells at passage 1, all recipient mice ($n = 6$) injected with cells from passage 16 developed tumors within 1 month (Fig. 1D).

NGS analysis identified the number of sgRNA pairs in cells or tumor samples; a higher number of pairs indicated a greater contribution to growth advantage; the original data were shown in table S1. We focused on candidate genes whose sgRNA appeared in both cell growth screening and nude mouse allograft tumors (Fig. 1E). *p53* ranked first in the candidate list in the presence of all six sgRNAs in the screening. This was followed by 22 other genes, whose sgRNAs appeared as one to three pairs, including *Cul5*, A-kinase anchoring protein 10 (*Akap10*), 7-dehydrocholesterol reductase (*Dhcr7*), and checkpoint kinase 2 (*Chk2*), these genes are related to p53 directly and indirectly (fig. S1C). Loss of *p53* has been reported to accelerate tumor formation in the *Brca1* deficiency background (*19*), and CHK2 regulates DNA damage repair via p53 and BRCA1 and promotes tumor formation in breast cancer (*20*–*22*). Thus, we considered *p53* and *Chk2* genes to be positive controls confirming that the screening generated reliable results. This analysis revealed that *Cul5* was a common candidate for SB screening and CRISPR-Cas9 screening (Fig. 1F).

Informatic analysis of The Cancer Genome Atlas database indicated that the expression level of CUL5 was decreased in human primary breast tumors ($n = 1097$) compared with that in normal tissues ($n = 114$) and that the expression level further decreased in metastatic tumors ($n = 7$; Fig. 1G). Further analysis of molecular subtypes of breast cancer revealed substantially lower levels of CUL5 in Basal, Her2$^+$, Luminal A, Luminal B, and normal-like breast cancers (fig. S1D). Kaplan-Meier plot of 1010 patients with breast cancer also showed that breast cancer patients with lower levels of CUL5 have lower probability of survival than the patients with higher levels of CUL5 (Fig. 1H). These clinical data were consistent with our finding that *Cul5* deficiency promoted tumorigenesis in breast cancer; therefore, we chose *Cul5* as a candidate gene for further analysis.

Cul5 knockout partially suppresses cellular lethality caused by *Brca1* deficiency

Since we found that lentivirus infection of the CRISPR library in *Brca1*-deficient MEFs overcame the lethality of *Brca1* deficiency via enrichment of *Cul5*-sgRNAs in the surviving cells, *Cul5* deficiency might be involved in overcoming the lethality associated with *Brca1* deficiency. To examine this, we used an inducible *Brca1*-knockout embryonic stem (ES) cell line (*Brca1*$^{Flox11/-}$*;Cre-ERT2*), in which Cre-mediated recombination was controlled by 4-hydroxytamoxifen (4-HT), as illustrated in Fig. 2A. Acute knockout of *Brca1* by 4-HT treatment resulted in no alive *Brca1*$^{-/-}$ ES colonies among the 96 ES colonies analyzed (Fig. 2B and fig. S2A). By contrast, we observed 8.3% (8 of 96) of *Brca1*$^{-/-}$ ES colonies survived in *Cul5*-knockout (*Brca1*$^{Flox11/-}$*;Cre-ERT2;Cul5*$^{-/-}$) ES cells, respectively (Fig. 2B and fig. S2A). We have shown earlier that deficiency of several genes including p53 and ATM could also suppress lethality caused by *Brca1* deficiency (*4*, *12*–*14*). As a comparison, we also knocked out these two potent tumor suppressors and found that disruption of p53 and ATM resulted in 37.5 and 22.9% *Brca1*$^{-/-}$ ES colonies, respectively (Fig. 2B). These observations suggest that *Cul5* deficiency, although not as potent as *p53* deficiency or *ATM* deficiency, partially suppressed cellular lethality caused by *Brca1* deficiency. Similarly, *Cul5* knockout also partially suppressed the cellular lethality caused by acute knockdown of *Brca1* (sh*Brca1*) in the mouse mammary cancer cell line 4T1 (Fig. 2, C and D, and fig. S2B). These data indicate that *Cul5* knockout partially suppresses the lethality caused by *Brca1* deficiency in different cell systems.

To further investigate the potential roles of *Cul5* deficiency in tumor growth, we knocked out *Cul5* in both *Brca1* WT (B447: *Brca1*$^{+/+}$*;p53*$^{-/-}$) and *Brca1* mutant (G600: *Brca1*$^{\Delta 11/\Delta 11}$*;p53*$^{-/-}$) cancer cells (*23*) and then evaluated growth rate under both in vitro and in vivo conditions. The results indicated that *Cul5* deficiency did not affect cell proliferation in different mammary

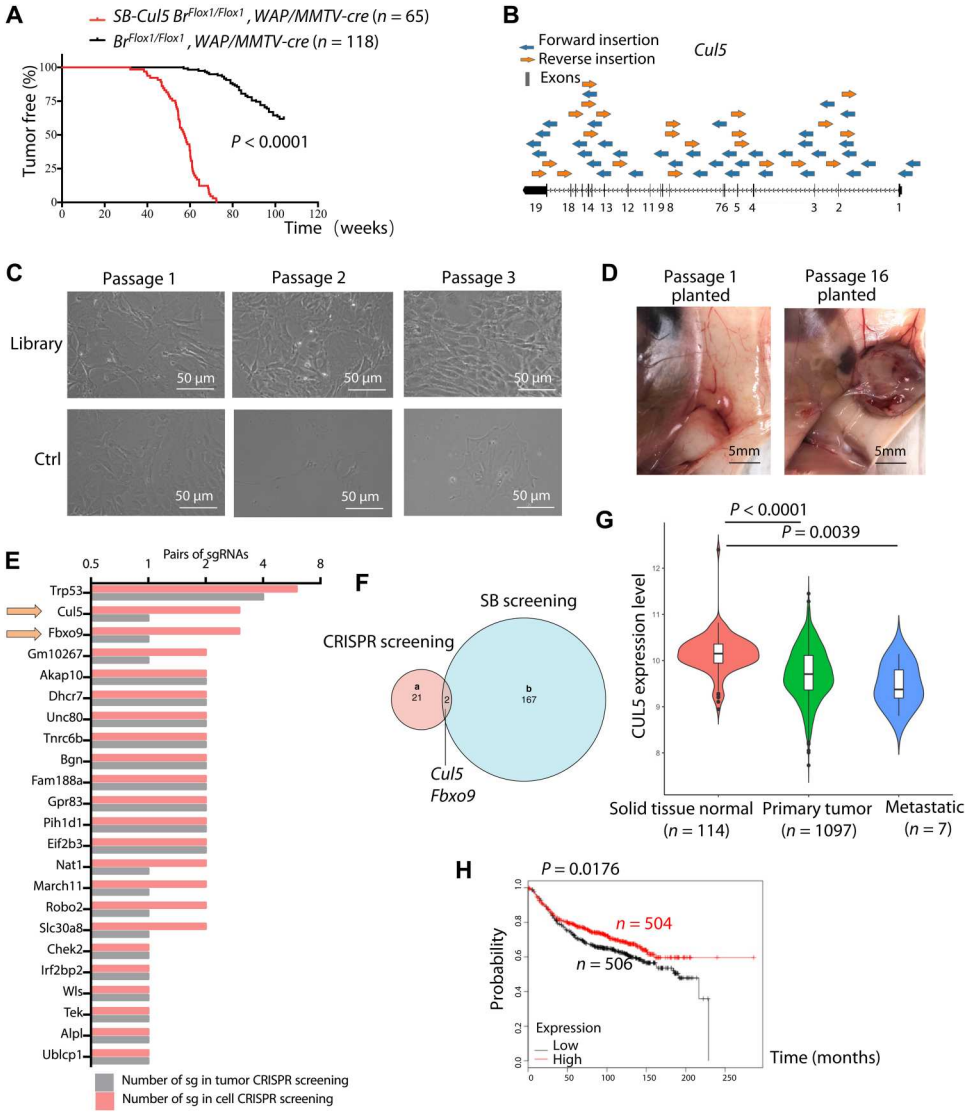

Fig. 1. Disruption of *Cul5* by sleeping beauty and CRISPR screening rescued *Brca1* lethality and triggered tumorigenesis. (**A**) Tumor-free curves of *Brca1*$^{Flox11/Flox11}$*;Wap-Cre or Brca1*$^{Flox11/Flox11}$*;MMTV-Cre* mice with or without SB transposon insertion in SB mice. $P \leq 0.0001$. (**B**) The SB transposon insertion sites and directions in the DNA sequence of *Cul5*. (**C**) Cell growth of MEFs after infection with a lentivirus-packaged mouse GeCKOv2 sgRNA library. Scale bars, 50 μm. (**D**) Representative photographs of primary tumors formed in nude mice transplanted with MEFs (passages 1 and 16) in fat pads. (**E**) Statistical analysis of sgRNA numbers that represent candidate genes appearing in both in vivo and in vitro screenings. (**F**) *Cul5* and *Fbxo9* were common candidate genes in CRISPR-Cas9 and SB screening. (**G**) The Cancer Genome Atlas statistics showing the mRNA expression level of CUL5 in normal mammary tissues, primary tumors, and metastatic tumors from patients with breast cancer. $P \leq 0.001$. (**H**) Kaplan-Meier plot showing the relationships between CUL5 expression and the probability of survival in 1010 human breast cancer patients (506 lower CUL5 and 504 higher CUL5).

cancer cell lines (Fig. 2, E to G) but accelerated tumor growth in tumors derived from both *Brca1*-WT B447 and *Brca1*-Mutant (MT) G600 cells, with a much stronger effect on the latter one (Fig. 2, H to J). Knockout of *Cul5* in these cells was confirmed by Western blotting and DNA sequencing (Fig. 2K and fig. S2C). Hematoxylin and eosin (H&E) staining showed that tumors with *Cul5* deficiency expressed higher levels of Ki-67 and lower levels of cleaved caspase-3 (Fig. 2, L and M).

We have tested *Brca1*-deficient HCC1937 cells (fig. S2, D and E) and *Brca1*-WT MDA-MB-231 cells (fig. S2, F to I). In HCC1937 cells, we transfected BRCA1 to make a pair of *Brca1*$^{-/-}$ and *Brca1*$^{+/+}$ isogenic cell lines. The data indicated that expression of BRCA1 completely suppressed tumor growth, whereas in both HCC1937 and HCC1937-BRCA1 cells, sg*Cul5* enhanced tumor growth (fig. S2, D and E). In MDA-MB-231 cells, we knocked down *Brca1* to make a pair of isogenic cell lines, and the data revealed that knockout of *Cul5* enhanced the xenograft tumor growth (fig. S2, E to I).

Overall, these data suggested that *Cul5* served as a tumor suppressor, and its deficiency promoted the initiation of *Brca1*-associated mammary tumorigenesis. Tumorigenesis may occur by overcoming the lethality effect caused by *Brca1* deficiency.

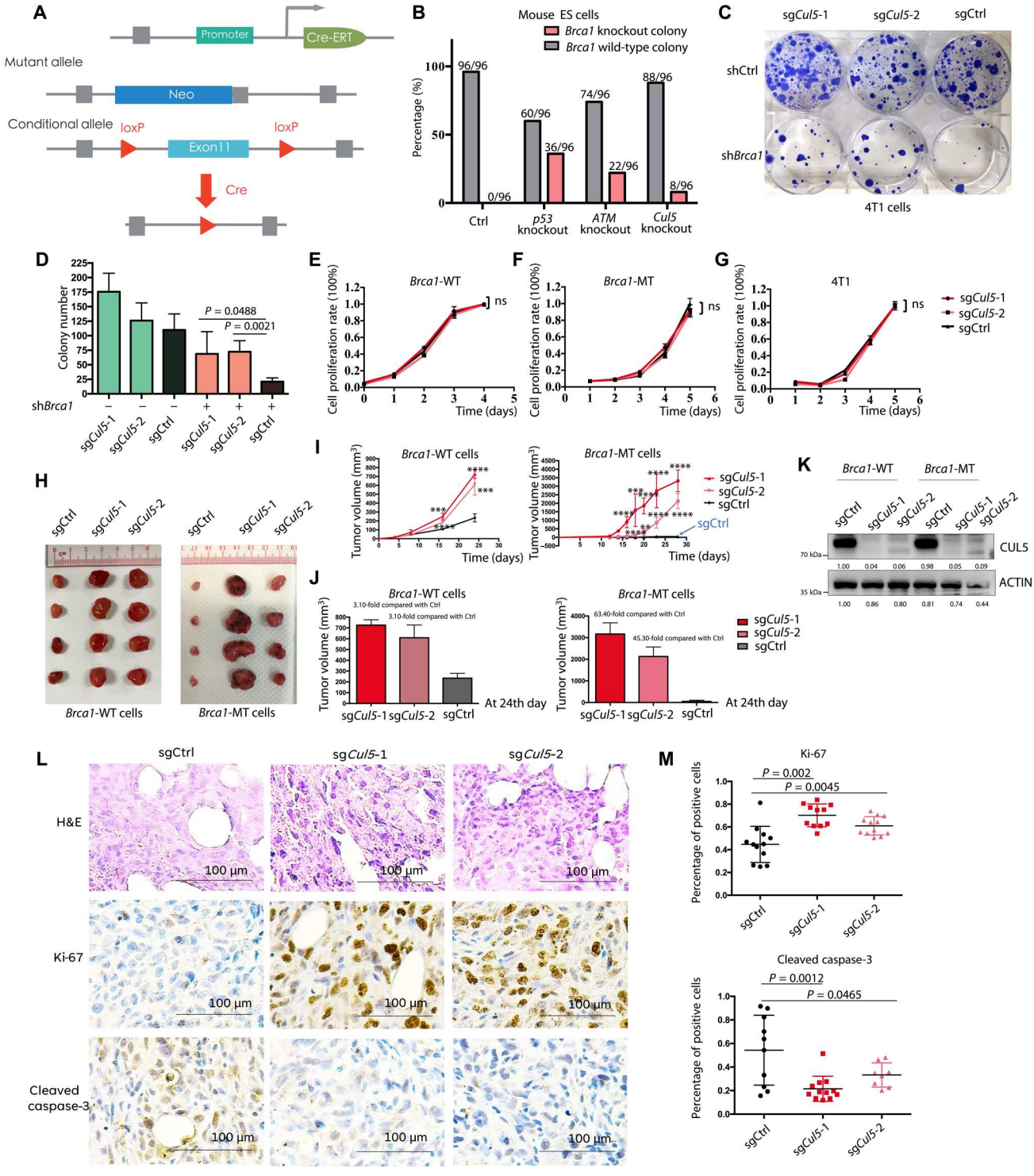

Fig. 2. *Cul5* deficiency rescued lethality caused by *Brca1* deficiency and accelerated tumor growth in breast cancer cells. (**A**) Schematic of inducible *Brca1*-knockout ES cell system. 4-HT treatment knocked out *Brca1* via CRE activation, leading to cell death via the apoptotic pathway. (**B**) Statistical analysis of the proportion of cells that rescued lethality caused by *Brca1* deficiency and remained viable by genotyping the *Brca1* exon 11 alleles using PCR. (**C**) Representative giemsa staining for observation of clonogenic cell growth in *Brca1*-knockdown 4T1 mammary tumors ($n = 3$). (**D**) Histogram showing the clonogenic cell growth of 4T1 cells ($n = 3$). (**E**) Cell growth curve of *Brca1*-WT cells with *Cul5* deficiency in vitro. (**F**) Cell growth curve of *Brca1*-mutant cells with *Cul5* deficiency in vitro. (**G**) Cell growth curve of 4T1 cells in vitro. (**H**) Comparison of implanted tumors in fat pads of nude mice ($n = 4$). (**I**) Tumor sizes at different time points ($n = 4$). *$P<0.05$, **$P<0.01$, ***$P<0.001$, and ****$P<0.0001$ by two sided Student's t test. (**J**) Tumor sizes at 24th hour ($n = 4$). (**K**) Western blot analysis of knockout efficiency in cancer cells. (**L**) Representative H&E, Ki-67, and cleaved caspase-3 immunostaining of primary tumors from nude mice derived from *Brca1*-mutant cells. (**M**) Quantification of positive cells in tumor samples from (L). ns, not significant.

Meanwhile, *Cul5* deficiency also promoted tumor development in *Brca1*-WT cells, although at a lower efficiency than in *Brca1*-MT cells, suggesting that CUL5 acts as a general tumor suppressor in breast cancer.

CUL5 orchestrated the TME to regulate tumorigenesis

The above results revealed that *Cul5*-knockout (KO) cells showed the similar proliferation rate as WT cells; however, *Cul5*-KO tumors developed much faster than *Cul5*-WT tumors (Fig. 2, H and I). These data suggested that the TME might be involved in promoting the growth of *Cul5*-KO tumors. To investigate this issue, we knocked out *Cul5* in 4T1 cells, which form tumors in immune-intact BALB/c mice, the knockout efficiency was shown in Fig. 3A. Tumors formed by 4T1-sg*Cul5* cells were substantially larger than those formed by parental 4T1 cells in allograft models, the tumor sizes were shown in Fig. 3B and tumor weights were shown in Fig. 3C. To elucidate the differences in the TME between *Cul5*-KO and *Cul5*-WT tumors, we applied cytometry by time of flight (CyTOF) to profile immune cell populations. The results showed that innate immune cell types, particularly monocytes and polymorphonuclear myeloid–derived suppressor cells (P-MDSCs), increased markedly in *Cul5*-KO tumors. Figure 3D shows the t-Distributed stochastic neighbor embedding (TSNE) results, and Fig. 3E shows the statistical analysis of the immune cell types. We also noticed that the increase in P-MDSCs was accompanied by a decrease in T cells (Fig. 3F), creating a favorable TME for tumor growth. Thus, we concluded that *Cul5* deficiency led to recruitment of monocytes and P-MDSCs to promote in vivo tumorigenesis.

To further confirm these immune changes, we checked monocytes and P-MDSCs in tumor sections using the markers CD11b and Ly6G. Notably, *Cul5*-deficient tumors showed much more positive signals than WT tumors, indicating the aggregate accumulation of immune cells, including P-MDSCs (Fig. 3, G and H). We also tested the mRNA levels in these tumor samples mixed with immune populations, and the results showed increase of monocyte and P-MDSC markers, such as Ly-6G, CCL2, CCR2, etc. (fig. S3A). To exclude the system interference in 4T1 cells, we induced *Cul5* deficiency into EMT6 cells, which is another typical mammary cancer cell line applied in immunology studies for breast cancer (*24*). The results showed similar phenomenon with that in 4T1 system (fig. S3, B to F), which indicates that *Cul5* deficiency alters the TME and triggered tumorigenesis regardless of the cell types.

Cul5 deficiency promoted the secretion of cytokines to regulate the TME

To further study TME changes in *Cul5*-deficient tumors, we digested the tumors and picked the single immune or tumor cells for further single-cell RNA sequencing (scRNA-seq). The results profiled immune cell subsets of about 230 cells from 18 mouse tumors with sgCtrl or sg*Cul5*. The uniform manifold approximation and projection (UMAP) cluster result showed natural killer (NK) cells, NKT cells, B cells, mast cells, endothelial cells, and innate lymphoid cells (Fig. 4A and fig. S4A). We further identified the proportion of each subtype by heatmap analysis (Fig. 4B) and pie plot analysis via the gene expression patterns (Fig. 4C). The results revealed several subtypes, including monocytes, macrophages, CD4-positive T cells, CD8-positive T cells, B cells, and stromal cells (fig. S4B). Consistent with the results in Fig. 3, knockout of *Cul5* markedly enhanced the numbers of monocytes and macrophage cells and suppressed the number of T cells (fig. S4C). As the monocytes are the initiatory altered immune cells dominating other immune subtypes, we analyzed the gene expression difference in monocytes with or without *Cul5* deficiency (Fig. 4D). *Cul5* knockout group showed higher expression of the genes involving regulation of cytokine production, cytokine-mediated signaling pathway, and the neutrophil degranulation (Fig. 4E). This result indicates that *Cul5* knockout recruits the monocytes by disturbing their cellular expression patterns, the signaling is transduced by secreted cytokines (*25*).

To investigate the possible causes of these TME changes in *Cul5*-deficient tumors, we conducted transcriptome analysis of 4T1 cells to study the downstream pathways of CUL5 (Fig. 4F). Gene set enrichment analysis (GSEA) indicated that the proteasome pathway was enriched in *Cul5*-deficient samples, which may serve as the negative feedback in response to *Cul5* deficiency (Fig. 4G and fig. S4, D and E). The chemokine signaling pathway was also enriched in *Cul5*-deficient samples (Fig. 4H). The heatmap further showed that some cytokines were induced upon *Cul5* deficiency; these cytokines included tumor-released monocyte chemoattractant protein 2 (CCL2), C-C motif chemokine ligand 5 (CCL5), C-X-C motif chemokine ligand 10 (CXCL10), and CXCL5 (Fig. 4I). These results were confirmed by gene expression analysis using reverse transcription polymerase chain reaction (RT-PCR) in three different mammary cancer cell lines (Fig. 4J), increase of CCL2 is the most obvious in *Cul5* knockout group compared to WT group. Previous studies have reported that monocytes are recruited mainly by CCL2 (*26*, *27*), and recruitment also involves CCL5 (*28*, *29*), CXCL10 (*30*, *31*), and CXCL5 (*32*, *33*). Thus, the increase of these cytokines may be responsible for the recruitment of monocytes in TME.

CUL5 ubiquitylates and degrades CREB1, especially under protein damage condition

Because CUL5 functions as a ubiquitin ligase scaffold protein, we next conducted a proteomic assay to identify proteins that are mainly regulated by CUL5 (Fig. 5A). In the isogenic pairs of G600-control and G600-sg*Cul5* cells, we found that cyclin-dependent kinase 13 (CDK13), TITIN (Connectin, TTN, which might be a common hit by mass spectrometry due to its large size), and CREB1 showed the highest fold changes among the isogenic pair of cells, suggesting that these proteins may be regulated by CUL5 (Fig. 5B; fig. S5, A and B; and table S2). Functional enrichment analysis by Metascape online tool indicated that these candidate proteins belonged to the protein-DNA complex assembly and regulation of binding (Fig. 5C). To further confirm the regulatory effects of CUL5, we validated the candidate protein level in allograft tumors. CREB1 showed the most obvious up-regulation in *Cul5*-deficient tumors (Fig. 5D). Similarly, we evaluated the expression correlation between CUL5 and CREB1 using an SB tumor tissue microarray. Higher expression of CREB1 was detected in the *Cul5*-deficient group (Fig. 5, E and F), indicating that the expression level was highly related to CUL5 expression. Metabric assay shows that the CUL5 expression level was negatively related with the expression level of CREB1 (fig. S5C).

CREB1 is a classic transcriptional factor that participates in multiple cellular processes, such as cell survival, proliferation, neuronal development, cell migration, cancer, and inflammation (*34*). Notably, in clinical studies, CREB1 has been shown to be both

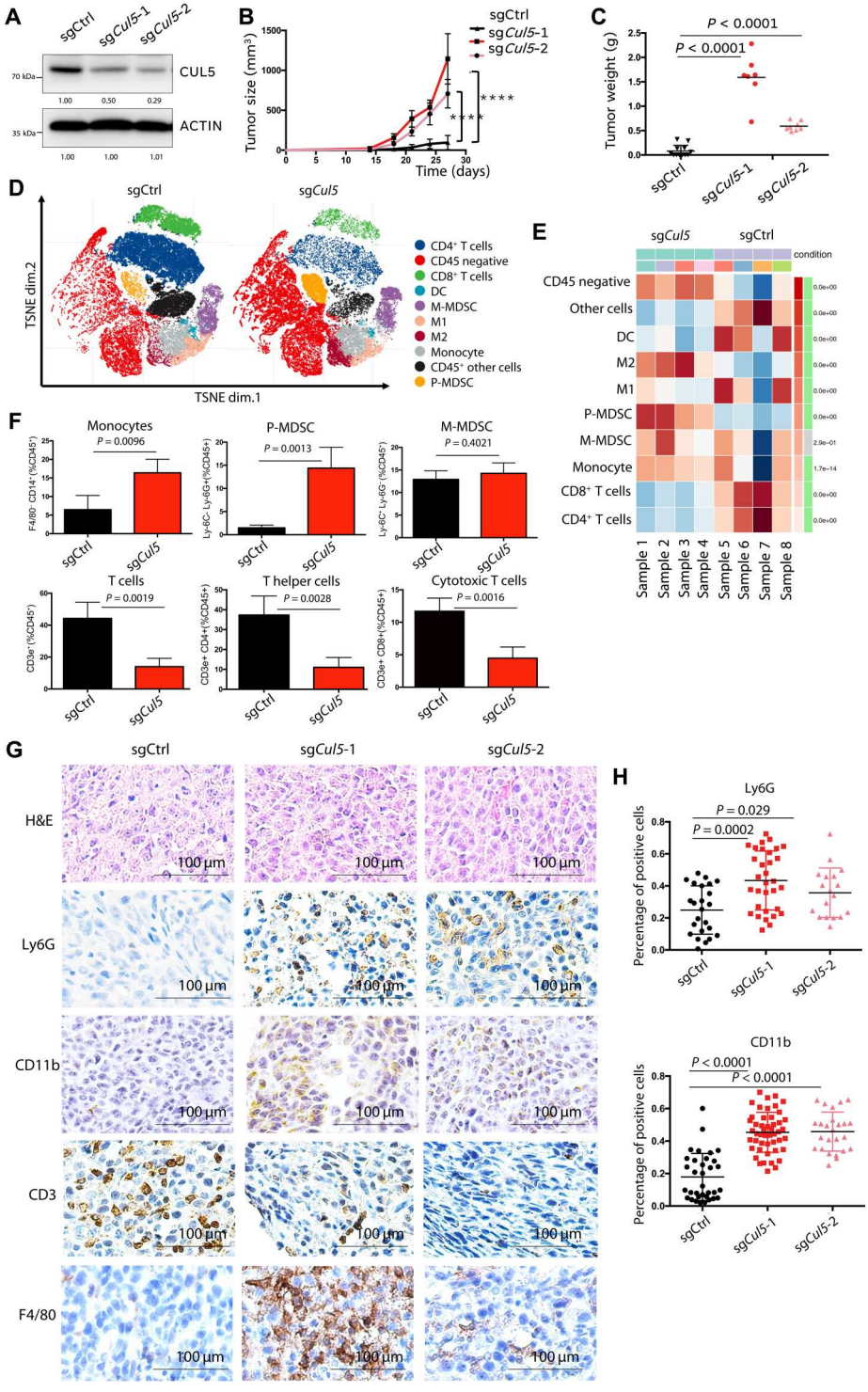

Fig. 3. *Cul5* deficiency disrupted the TME and promoted monocytes and P-MDSC. (**A**) Western blot analysis of CUL5 expression in 4T1 cells with *Cul5* deficiency. (**B**) Tumor size ($n = 8$) of xenografts in fat pads implanted with 4T1 cells with *Cul5* deficiency. (**C**) Tumor weight ($n = 8$) of xenografts in fat pads implanted with 4T1 cells. (**D**) TSNE results of CyTOF assays to analyze immune subtypes ($n = 4$). (**E**) The proportion of each immune subtype in all eight samples. (**F**) Histogram showing a summary of immune cell changes for each cell subtype ($n = 4$). (**G**) Representative immunohistochemical results showing immune markers in *Cul5*-knockout tumors samples. (**H**) Quantification of positive cells in *Cul5*-knockout tumor samples.

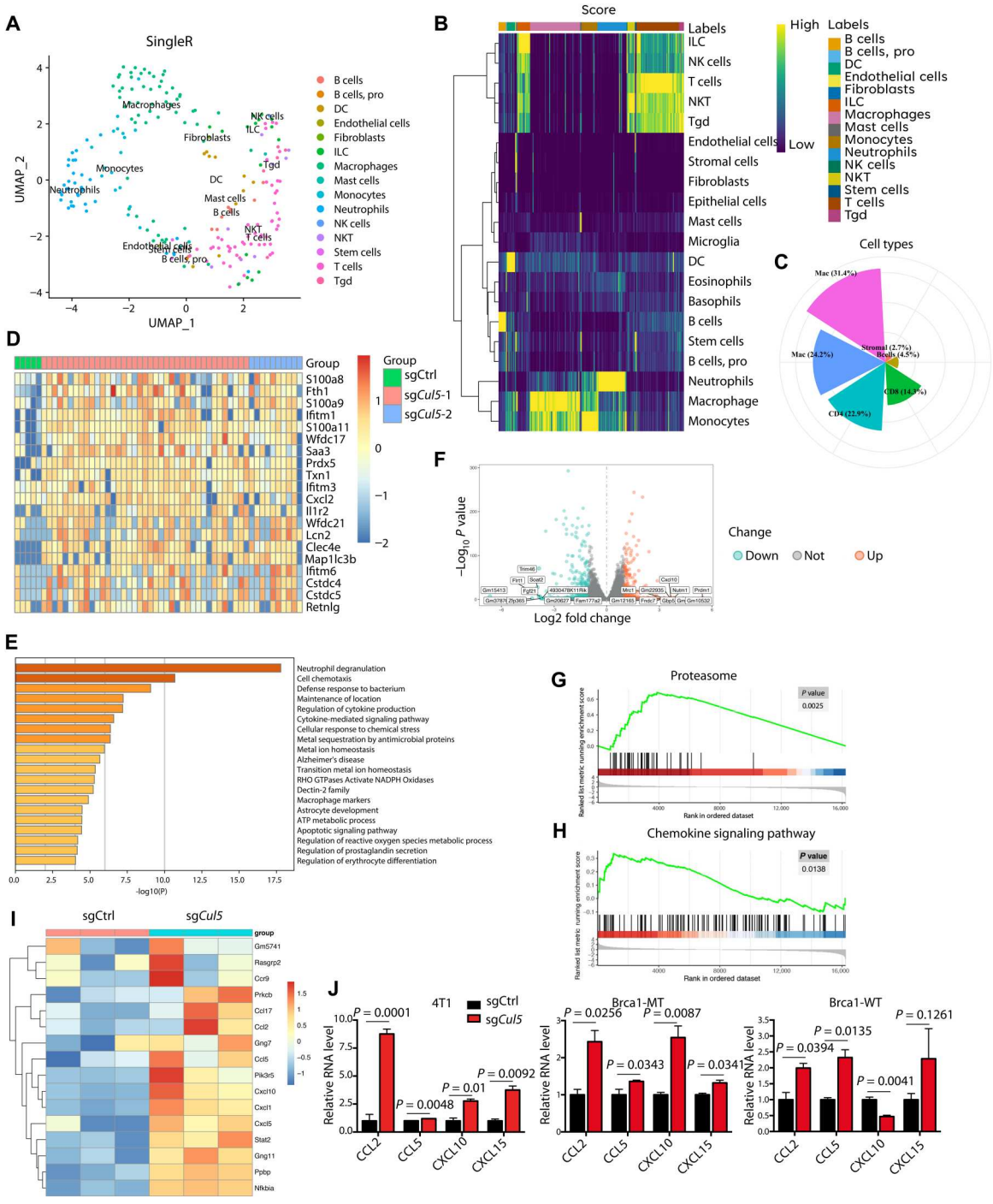

Fig. 4. *Cul5* deficiency promoted chemokine signaling pathway activation. (**A**) UMAP plot showing integrated immune cell clusters from sgCtrl and sg*Cul5* tumors. The results profiled immune cell subsets of about 230 cells from 18 mouse tumors with sgCtrl or sg*Cul5*. (**B**) Heatmap of phonograph clusters of immune cells; rows represent different clusters of single cells. DC, dendritic cell, ILC, innate lymphoid cells, Tgd, T gamma delta immune cells. (**C**) Pie plot showing the cell types and their proportions among the immune populations. (**D**) Heatmap of gene expression patterns of monocytes; rows represent clusters of single cells grouped by different sgRNA treatments to knockout *Cul5*. (**E**) Up-regulated pathways of monocytes in *Cul5* knockout groups compared with *Cul5* wide-type group. (**F**) Volcano plot of RNA-seq gene expression changes due to *Cul5* deficiency in 4T1 cells (n = 3). (**G**) Gene set enrichment analysis (GSEA) revealed up-regulated chemokine signaling pathway in *Cul5*-knockout cells. NES, normalized enrichment score; $P < 0.05$. (**H**) GSEA revealed proteasome pathway in *Cul5*-knockout cells. $P < 0.05$.(**I**) Relative mRNA level of genes in the chemokine pathway in 4T1 cells with *Cul5* deficiency, as determined by RNA-seq (n = 3). (**J**) Relative mRNA levels of several cytokines in 4T1, mammary cancer cell line with mutant *Brca1* (G600), and mammary cancer cell line with WT *Brca1* (B477) (n = 3).

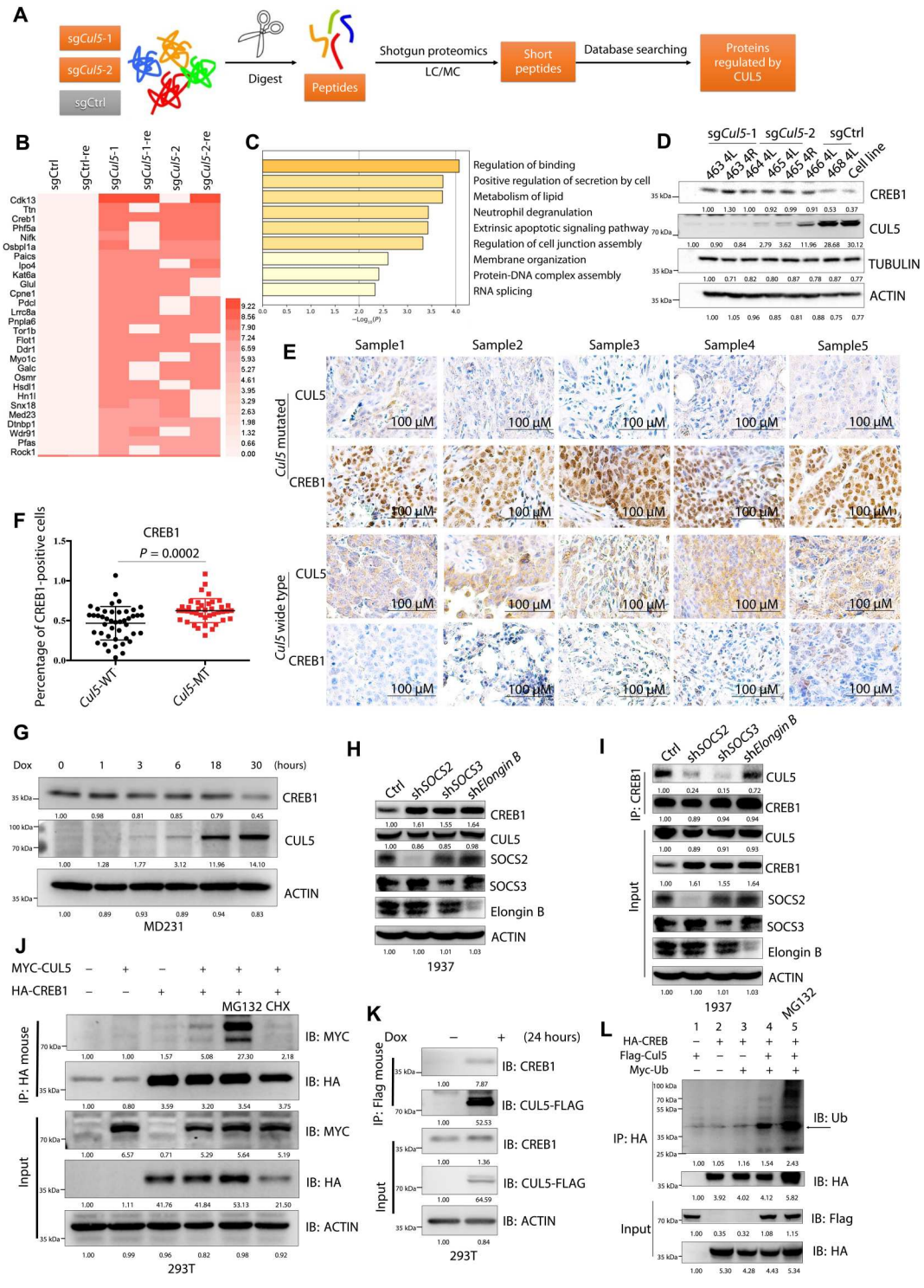

Fig. 5. Accumulation of CREB1 was related to *Cul5* deficiency. (**A**) Schematic of proteomics analysis by the shotgun method. LC/MC, Liquid Chromatograph Mass Spectrometer. (**B**) Up-regulated proteins in *Cul5*-deficient mammary cancer cells, as determined by mass spectrum analysis. The sample marked "re" is the biological duplicate. (**C**) Up-regulated pathways in *Cul5*-deficient mammary cancer cells according to the candidate score in (B) by metascape online tool. (**D**) Western blot analysis of the up-regulated candidate proteins in *Cul5*-deficient tumors. (**E**) Representative immunohistochemical staining of CUL5 and CREB1 in mouse SB tumors with *Cul5* deficiency. (**F**) Calculated percentage of CREB1-positive cells in *Cul5*-WT or *Cul5*-mutant SB samples (n = 43 and 40, respectively). (**G**) Western blot results of MDA-MB-231 human breast cancer cells in the Tet-On system. Dox, doxycycline (1 μg/ml). (**H**) Western blot analysis of the related proteins in HCC1937 cells with knockdown of SOCS2, SOCS3, or Elongin B. (**I**) Immunoprecipitation (IP) assays showing the interaction of endogenous CREB1 and CUL5 in HCC1937 cells with knockdown of SOCS2, SOCS3, or Elongin B. (**J**) Immunoprecipitation assays showing the interaction of overexpressed CREB1 and CUL5 in 293T cells. MG132, 10 μM, 6 hours. CHX, cycloheximide, 10 μM, 6 hours. (**K**) Immunoprecipitation assays showing the interaction between CUL5 overexpression and endogenous CREB1 expression in 293T cells. IB, immunoblot. (**L**) Immunoprecipitation assays showing the ubiquitination of CREB1 with Cul5 expression and treatment of MG132, 10 μM for 7 hours. Ub, ubiquitination.

up-regulated and constitutively phosphorylated in patients with acute myeloid leukemia and non–small cell lung cancer (*35*). To further confirm the correlation between CREB1 and CUL5, we used a Tet-On system to induce CUL5 overexpression in multiple mammary cancer cell lines. Overexpression of CUL5 decreased the protein level of CREB1 in a time course study (Fig. 5G and fig. S5D). We also tested previously identified substrates or downstream proteins of CUL5, such as TANK-binding kinase 1 (TBK1), snail family transcriptional repressor 2 (SNAI2), and MAPK associated protein 1 (SIN1), knockout of *Cul5* increased the expression of TBK1, SNAI2, and SIN1 along with CREB1 (fig. S5, E and F). These data suggest that CREB1 is one of the main downstream proteins of the CUL5. According to previous publications (*36*), we checked suppressor of cytokine signaling (SOCS)-box

adaptor proteins that may be involved in Cul5-CREB1 axis, including SOCS2, SOCS3, and Elongin B. The data indicated that knockdown of these proteins increases the level of CREB1 (Fig. 5H), and knockdown of *SOCS2* or *SOCS3*, but not *Elonbin B*, interferes interaction between CREB1 and CUL5 (Fig. 5I). These data suggest that SOCS2 and SOCS3 play a more critical role in CUL5 and CREB1 interaction than Elongin B, although it might be involved in the stabilization of CREB1.

To confirm the physical contact between CREB1 and CUL5, we detected the interactions of these proteins using immunoprecipitation analysis. CREB1-human influenza hemagglutinin (HA) and CUL5-Flag were overexpressed in 293T cells. Anti-HA antibody was used to immunoprecipitated CREB1-HA, and CUL5 was detected by immunoblotting. The results demonstrated that this interaction occurred and could be enhanced by MG132 and suppressed by cycloheximide (Fig. 5J). Similar results were confirmed using immunoprecipitation of Flag-CUL5 with immunoblotting for endogenous CREB1 (Fig. 5K and fig. S5I). Consistent with our finding that CUL5 deficiency increase the CREB1 protein level, our data indicated that CUL5 ubiquitylates CREB1, and the ubiquitination could be further enhanced by MG132 (Fig. 5L). We have shown previously that that many therapeutic drugs could damage protein, and the damaged proteins were ubiquitinated and degraded by proteosomes (*37*). To test whether CREB1 could be damaged and degraded upon the treatment of therapeutic drugs, we treated cells with cinacalcet hydrochloride, which is a U.S. Food and Drug Administration–approved drug for chronic kidney disease and parathyroid carcinoma. The data indicated that it induced strong protein damage and caused ubiquitination of CREB1 (fig. S5, J and K). Together, these data showed that CREB1 is previously unidentified substrate of CUL5; meanwhile, we found that ubiquitination was substantially enhanced under the protein damage condition.

CUL5 regulated CREB1 expression to facilitate the reprograming of the TME

A recent study showed that CREB1 could regulate CCL2 through transforming growth factor–β2 (TGF-β2) (*38*). Therefore, we speculated that CUL5 might act through CREB1 to mediate the formation of the TME and thereby promote tumorigenesis. To investigate this, we knocked out *Creb1* in *Cul5*-WT and *Cul5*-KO cells (Fig. 6A), followed by inoculation of the cells into mice to monitor tumorigenesis. We found that *Creb1* knockout abolished the tumor growth advantage of *Cul5*-KO cells (Fig. 6, B to E), suggesting that CREB1 might participate in tumor growth in *Cul5*-KO tumors and that higher expression levels of CREB1 in *Cul5*-KO cells might trigger tumor growth. Consistent with our previous results, we found that knockout of *Cul5* facilitated tumorigenesis, whereas *Creb1* deficiency abolished this effect. Meanwhile, we implanted the tumors in G600-Nude mouse system and achieved the similar results (fig. S6, A and B). To confirm *Creb1*'s contribution on tumor growth in 4T1-Balb/c system, we knocked out *Creb1* in front of *Cul5*; the phenomenon was quite similar as the Fig. 6A shows, which confirmed that *Creb1* deficiency could inhibit the tumorigenesis caused by Cul5 deficiency (fig. S6, C and D). To further validate the roles of CREB1 in *Cul5*-defective tumors, we processed the tumor samples using CyTOF assays (Fig. 6F). Same with the results in Fig. 3, *Cul5* deficiency promoted the recruitment of monocytes and P-MDSCs and further suppressed T cells, whereas knockout of *Creb1* in the *Cul5*-deficient background reversed these changes in the TME. *Creb1* knockout abolished the recruitment of monocytes and P-MDSCs induced by *Cul5* deficiency and increased T cell populations (Fig. 6G and fig. S6, E and F). These results indicate that CREB1 is the main downstream molecule of CUL5 in modulating the TME.

By detecting the expression patterns of CREB1 downstream genes, we found that knockout of *Cul5* enhanced the expression of CREB1 target genes, such as estrogen receptor 1 (*ESR1*), vascular endothelial growth factor (*VEGF*), and brain-derived neurotrophic factor (*BDNF*), in *Brca1*-deficient and WT mammary cancer cells (Fig. 6, H and I). *Creb1* knockout reversed the expression patterns of ESR1, VEGF, and BDNF in *Cul5*-knockout mammary cancer cells (Fig. 6J). CREB1 binds to its DNA target sequence [i.e., the cAMP-responsive element (*CRE*)] and initiates gene expression (*34*). Our results showed that knockout of *Cul5* in *Brca1*-deficient mammary cancer cells also enhanced the CREB1 binding activity toward the CRE binding site by abolishing the CREB1 degradation process (Fig. 6K).

CREB1 has been reported to regulate many types of immune cells, both in adaptive and innate immune systems (*34*); for example, CREB1 has been found to recruit both monocytes and macrophages (*39*–*41*). In our study, we found that *Cul5* deficiency increased CREB1 protein levels, resulting in enhanced recruitment of immune cells, such as monocytes and macrophages, through its downstream cytokines, such as CCL2, CCL5, CXCL5, and CXCL10.

CCL2 is regulated by CUL5 and CREB1 to enhance the tumor growth

To validate the association of CCL2 with CUL5 and CREB1 in tumorigenesis, we knocked out *Ccl2* in *Cul5*-WT and *Cul5*-KO cells (Fig. 7A) followed by inoculation of the cells into BALB/c mice for tumorigenesis. We found that *Ccl2* knockout abolished the tumor growth advantage of *Cul5*-deficient cells (Fig. 7, A to C), indicating that CCL2 might participate in the growth of *Cul5*-KO tumors and that higher expression levels of CREB1 in *Cul5*-KO cells might trigger tumor growth. Consistent with our previous results, we found that knockout of *Cul5* facilitated tumorigenesis, whereas *Ccl2* deficiency abolished this effect. To further validate the role of CCL2 in *Cul5*-deficient tumors, we extracted the proteins and mRNA of the tumor samples. It shows that knockout of *Cul5* increased the expression level of CCL2 (Fig. 7, D and E). Meanwhile, knockout of *Creb1* in *Cul5*-deficient 4T1 cells reduced the expression level of CCL2 (Fig. 7F), which is consistent with previous publication that CREB1 positively regulates the expression and secretion of CCL2 (*38*). Our results suggest that *Cul5* deficiency enhances tumorigenesis in mammary cancer mainly through CREB1 and CCL2, and CCL2 is also regulated by CREB1.

A CREB1 inhibitor blocked the TME to promote successful tumor treatment

CUL5 functions as a tumor suppressor in breast cancer, and its expression often remains at a relatively low level in clinical tumor samples. Activation of CUL5 or inhibition of downstream activities may have applications in the treatment of cancers with low levels of CUL5. However, in a literature search, we found no suitable agonist for activating CUL5; thus, we focused on 666-15, an inhibitor of CREB1. We found that this compound, under in vitro condition, had a moderate inhibitory effect on *Brca1*-WT 4T1 cells but elicited a much stronger effect on *Brca1*-MT G600 cells (Fig. 8, A and B). To

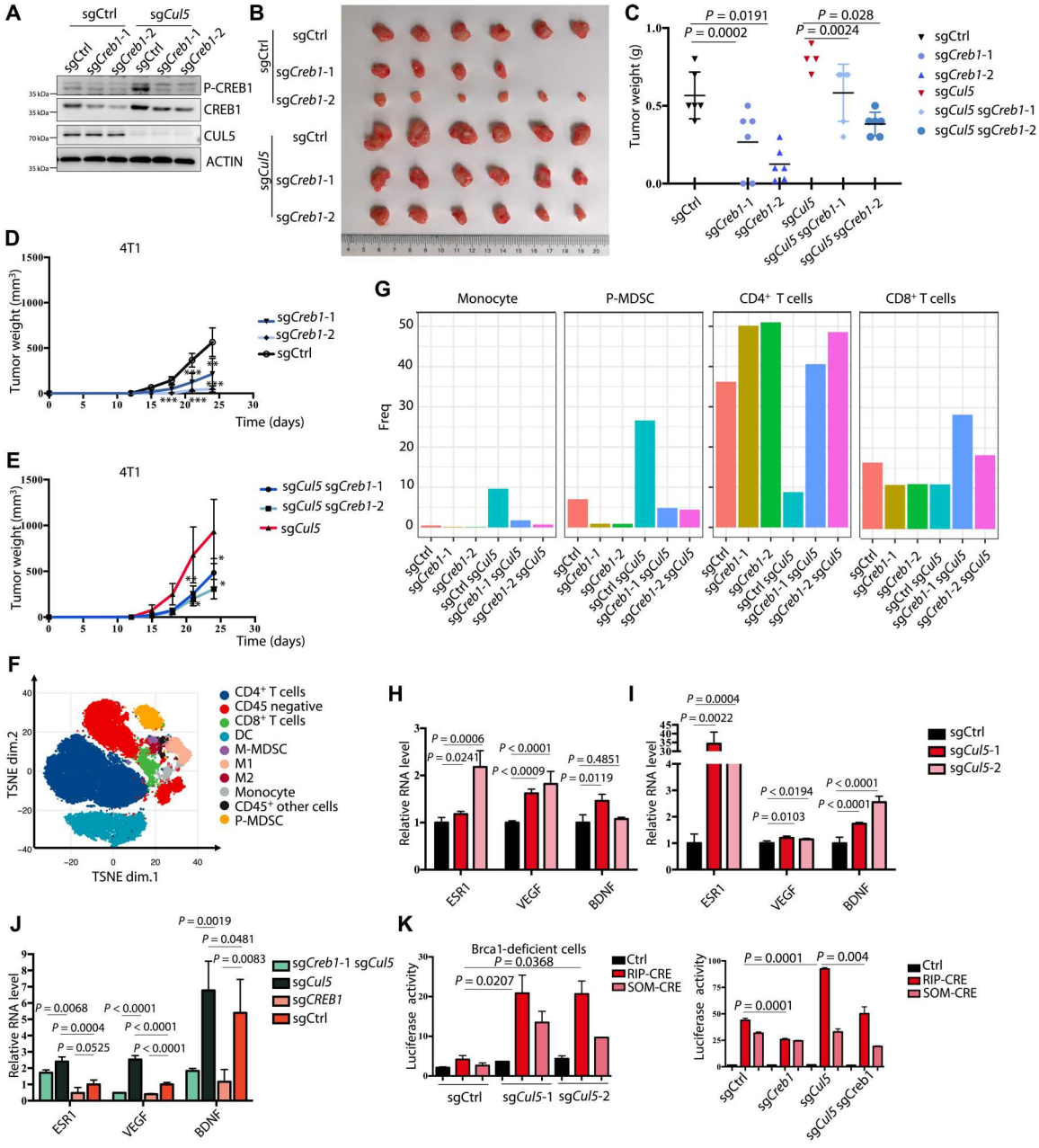

Fig. 6. *Creb1* deficiency reversed the effects of *Cul5* deficiency. (**A**) Western blot analysis to confirm the knockout efficiency in 4T1 cells. (**B**) Photograph showing tumor size ($n = 8$) of xenografts in fat pads implanted with 4T1 cells with *Cul5* and *Creb1* deficiency. *Cul5* was knocked out first, following by *Creb1* knockout. (**C**) Tumor weight ($n = 8$) of xenografts in fat pads implanted with 4T1 cells. (**D**) Tumor growth curves ($n = 8$) of xenografts in fat pads implanted with 4T1 cells with WT *Cul5*. (**E**) Tumor growth curves ($n = 8$) of xenografts in fat pads implanted with 4T1 cells with *Cul5* deficiency. (**F**) TSNE results of CyTOF assays for analysis of immune cell subtypes ($n = 6$). (**G**) The proportion of each immune cell subtype in *Cul5*- or *Creb1*-deficient tumors. (**H**) Relative mRNA levels of target genes in *Brca1*-deficient mammary cancer cells with *Cul5* deficiency ($n = 3$). (**I**) Relative mRNA levels of target genes in *Brca1*-WT mammary cancer cells with *Cul5* deficiency ($n = 3$). (**J**) Relative mRNA levels of target genes in *Brca1*-deficient mammary cancer cells with *Cul5* and *Creb1* deficiency. (**K**) Relative luciferase activity of CRE in *Brca1*-deficient mammary cancer cells with *Creb1* and *Cul5* deficiency. RIP-CRE, the active form of CRE; SOM-CRE, the inactive mutant of CRE.

confirm whether the drug works well in vivo, we injected 4T1 and 4T1-sg*Cul5* cells into BALB/c mice. The data indicated that tumors derived from 4T1-sg*Cul5* cells grew much faster than 4T1 parent cells, consistent with our earlier observation that CUL5 acted as a tumor suppressor (Fig. 8C). Treatment with 666-15 nearly completely reversed the tumor growth caused by *Cul5* deficiency, as determined by measurement of tumor weight (Fig. 8C) and size (Fig. 8, D and G) and cell proliferation (Fig. 8H). Immunohistochemistry using markers for various immune cell types also showed that 666-15 treatment reversed the TME caused by *Cul5* deficiency (Fig. 8I). We have also treated 4T1-sh*Brca1*, 4T1-sg*Cul5*, 4T1-sg*Cul5* + sh*Brca1*, and 4T1-sgCtrl cell lines with 666-15, and

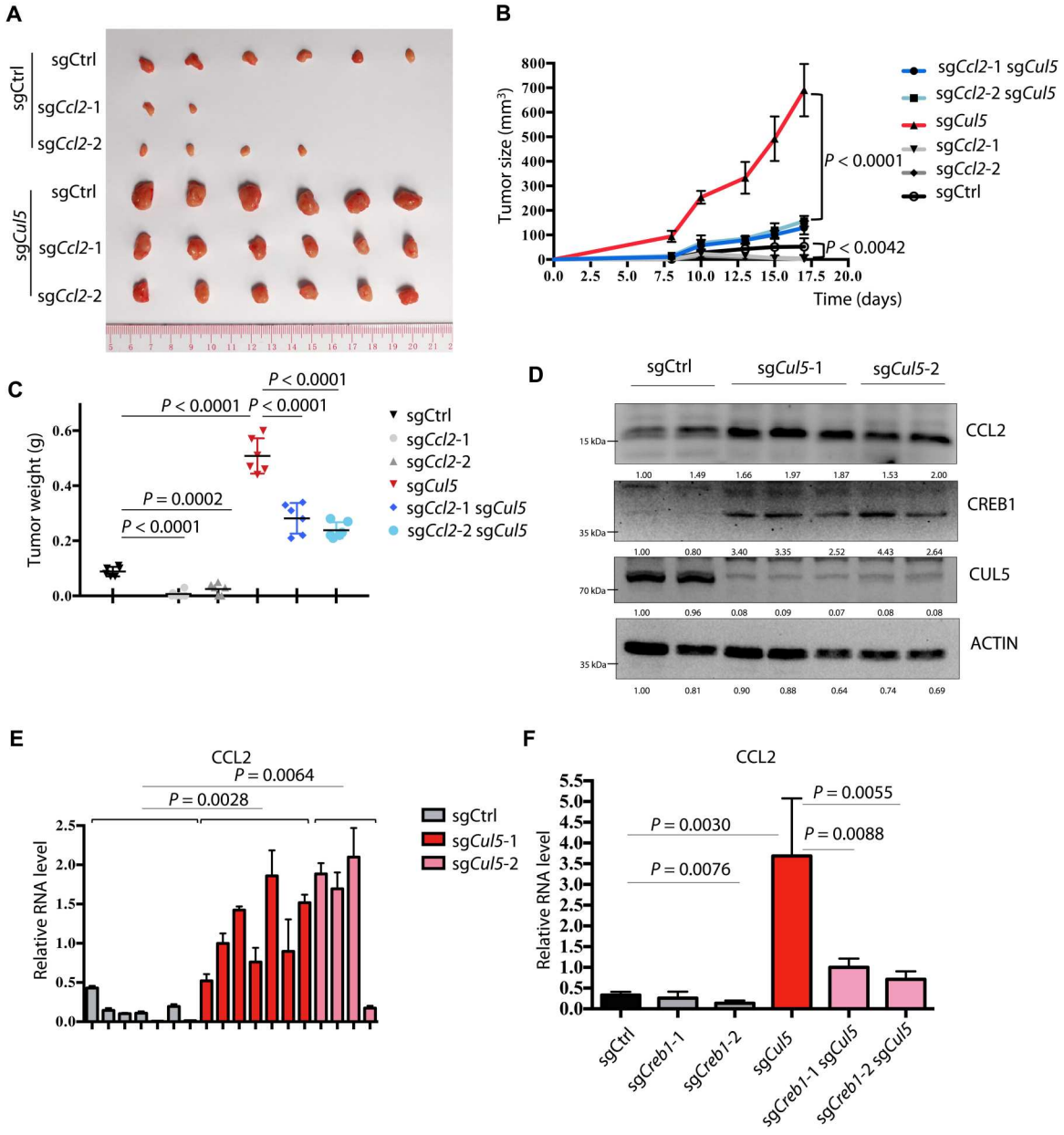

Fig. 7. *Ccl2* deficiency reversed the effects of *Cul5* deficiency. (**A**) Photograph showing tumor ($n = 6$) of xenografts in fat pads implanted with 4T1 cells with *Cul5* and *CcL2* deficiency. *Cul5* was knocked out first, following by *CcL2* knockout. (**B**) Tumor growth curves ($n = 6$) of xenografts in fat pads implanted with 4T1 cells with WT-*Cul5*. (**C**) Tumor weight ($n = 6$) of xenografts in fat pads implanted with 4T1 cells. (**D**) Western blot analysis to confirm the expression level of CCL2 in tumors. (**E**) Relative mRNA levels of target genes in *Brca1*-deficient mammary cancer cells with *Cul5* deficiency ($n = 3$). (**F**) Relative mRNA levels of target genes in *Brca1*-deficient mammary cancer cells with *Cul5* and *Ccl2* deficiency ($n = 3$).

the data showed that 666-15 substantially inhibited the *Brca1* mutant cell growth and tumorigenesis (fig. S8).

In summary, our findings in this study showed that 666-15 treatment rescued *Cul5* deficiency by inhibiting the function of CREB1 in recruiting immune cells, such as monocytes and MDSCs. In summary, our studies identify that *Cul5* deficiency triggers tumor growth via TME equilibrium, causes the aggregation of monocytes and P-MDSCs, and leads to a decrease in the number of T cells. This phenomenon is reversed by knockout of *Creb1*, a substrate of the ubiquitin ligase CUL5. The 666-15, an inhibitor of CREB1, blocks tumor growth caused by *Cul5* deficiency (Fig. 8J).

DISCUSSION

In this study, we conducted sleeping beauty–mediated genome-wide screening in *Brca1*-deficient cells and mouse models to identify the possible synergic genes whose deficiency may accelerate *Brca1*-associated tumorigenesis. The results revealed that *Cul5* deficiency promoted tumor growth in *Brca1*-deficient mice, which

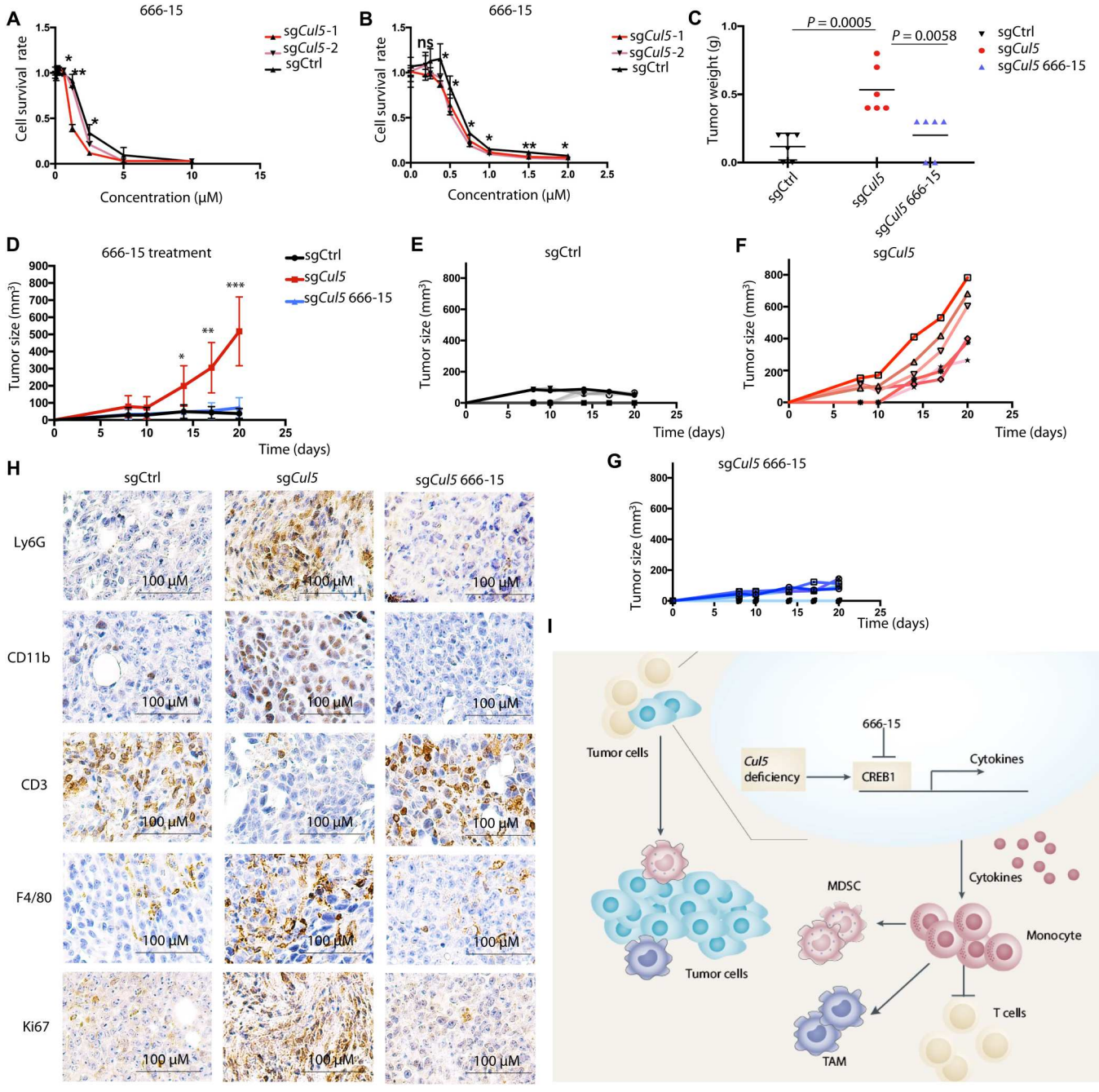

Fig. 8. Effects of CREB1 inhibitor treatment in *Cul5*-deficient tumors. (**A** and **B**) Cell survival rate with *Cul5* knockout (sg*Cul5*) following CREB1 inhibitor (666-15) treatment in 4T1 (*Brca1*-WT) cells (A) and G600 (*Brca1*-MT) cells. The 4T1 and G600 cells have quite different sensitivity toward the inhibitor, with half-maximal inhibitory concentration values of 2.15 and 0.68 μM, respectively. (**C**) Tumor weight ($n = 6$ for each group) of xenografts in fat pads implanted of 4T1 cells with *Cul5* deficiency and 666-15 treatment at day 20. 666-15, 10 mg/kg, once a day, 5 days/week. (**D**) Tumor volumes of 4T1-sgControl cells, 4T1-sg*Cul5* cells, and 4T1-sg*Cul5*/666-15. (**E** to **G**) Tumor volumes of 4T1-sgControl cells (E), of 4T1-sg*Cul5* cells (F), and 4T1-sg*Cul5*/666-15 treatment over time ($n = 6$ for each group). (**H** to **I**). Representative immunostaining with antibodies to Ki-67 (H) and immune cell markers, Ly6G, F4/80, and CD3 (I) of primary tumors from in vivo drug treatment assays. (**J**) Model summarizing *Cul5* deficiency as a master switch of the TME to mediate tumorigenesis in breast cancer via CREB1 and CCL2.

was subsequently confirmed by CRISPR-Cas9–mediated screening. During the tumor growth process, *Cul5* deficiency facilitated the recruitment of monocytes and P-MDSCs, which suppressed T cell populations and created a favorable TME for tumor growth. Moreover, the data also showed that CREB1 interacted with CUL5 and acted as a previously unidentified ubiquitination substrate of CUL5; the ubiquitination was enhanced under protein damage condition. When *Cul5*-deficient tumors were treated with the CREB1 inhibitor 666-15, their growth was inhibited. Thus, these findings may facilitate the development of previously unidentified treatments for breast cancer.

Monocytes are the largest type of leukocytes and can differentiate into myeloid lineage dendritic cells and macrophages (*42*). They are also important innate immune cells related to many cancer-associated procedures, such as immune tolerance, angiogenesis, metastatic spread, and chemotherapy resistance (*26*). Previous studies have shown that MDSCs affect tumorigenesis by linking inflammation and cancer; the plasticity of MDSCs either positively or negatively contributes to growth or metastasis in a yin-yang model (*43*). A study on pancreatic cancer showed that deletion of the gene encoding collagen type 1 leads to recruitment of MDSCs and suppression of CD8-positive T cells via increased CXCL5 in cancer cells (*44*). We also found that an increase in P-MDSCs led to a decrease in T cells. Thus, our findings support that *Cul5* deficiency promotes the recruitment of monocytes to the tumor region, enabling the construction of an immunosuppressive microenvironment for tumor growth.

CCL2 recruits inflammatory monocytes to promote tumor metastasis in breast cancer (*45*). The CCL2/CCR2 signaling axis has attracted much interest in recent years owing to its relationships with tumorigenesis (*26*, *46*). Inhibition of the CCL2/CCR2 axis attenuates monocyte aggregation in a mouse mammary cancer model and reduces tumorigenesis and metastasis (*45*, *47*). Moreover, *Ccr2*$^{-/-}$ mice show fewer circulating monocytes (*48*, *49*). Inhibition of CCL2 by oral administration of bindarit suppresses inflammatory monocyte infiltration and alters macrophage populations (*50*). Furthermore, in this study, we found that *Cul5* deficiency increased the levels of several cytokines, including CCL2, CCL5, CXCL5, and CXCL10, which are known to play various roles in recruiting monocytes (*26*–*33*). Therefore, we believe that up-regulation of these cytokines is responsible for the formation of a tumor immunesuppressive microenvironment.

Several previous studies have also found decreased levels of CUL5 in different cancer cells, including lung cancer cells and ovarian cancer cells (*51*, *52*). Recently, one group reported that the absence of CUL5 triggers metastasis in small cell lung cancer and that *CUL5* deficiency inhibits the degradation of integrin β1, leading to the aggregation of integrin β1. *CUL5* deficiency promotes focal adhesion kinase/SRC signaling and enhances metastasis. Moreover, they showed that the CUL5 and integrin β1 genes were involved in the formation of small cell lung cancer (*53*). Another team reported that *CUL5* functions as a previously unidentified candidate tumor suppressor in renal cell carcinoma by preventing DNA damage and participating in DNA double-strand break repair (*54*). Other reports have provided limited evidence that CUL5 participates in the signal transducer and activator of the transcription/Janus kinase 2 pathway (*55*), is involved in the phosphorylation of mitogen-activated protein kinase (MAPK) and p53 (*56*), regulates the function of gp130 signaling (*57*), and degrades the Dishevelled, EGL-10 and pleckstrin (DEP) domain–containing mammalian target of rapamycin (mTOR)–interacting protein (DEPTOR) to regulate the mTOR pathway (*52*, *58*). However, very little is known regarding the functions of CUL5 in the tumorigenesis of breast cancer.

In this study, we found that CUL5 expression levels were obviously decreased in human primary breast cancers compared with that in normal tissues and were further decreased in metastatic tumors. We found that breast cancer patients with lower levels of CUL5 have lower probability of survival than patients with higher levels of CUL5. We have also compared CUL5 expression in human triple-negative breast cancer (TNBC) versus non-TNBC and *Brca1*$^{-/-}$ versus B*rca1*$^{+/+}$ breast cancers, and there are no obvious differences in these comparisons. These data indicated that like its role in several other type of cancers; CUL5 may also serve as a breast tumor suppressor. Regarding to its relationship with BRCA1, our functional analyses demonstrated that Cul5 deficiency markedly enhances *Brca1*-associated tumorigenesis. We have previously demonstrated that *Brca1* deficiency does not directly cause tumorigenesis; instead, it results in cellular growth defects duo to genetic instability, and the tumorigenesis could occur after some further changes, including inactivation of tumor suppressors (such as p53 and ATM) (*4*, *12*–*14*) and activation of oncogenes (such as *ER*α signaling and *Notch1*) (*16*, *23*, *59*). Our further analysis indicated that loss of CUL5 ubiquitin ligase activity enables the *Brca1* mutant cells to overcome the cellular growth defects and proliferation. While *Cul5* deficiency supports tumor growth of both *Brca1*-WT and *Brca1*-MT cancers, *Cul5* elicits much higher efficiency for the *Brca1*-MT cancer. Thus, our data reveal that CUL5 not only serves as a general tumor suppressor but also plays an important role for BRCA1-associated tumorigenesis, highlighting its important role for breast cancer research.

The ubiquitin-proteasome system is responsible for posttranslational modifications that are required for many biological processes, such as protein degradation, cell cycle processes, translational regulation, signal transduction, and DNA repair (*60*). These processes are involved in the homeostasis of tumor suppressors and oncoproteins. CUL5 interacts with the ring finger protein 7 (RNF7), SOCS box proteins, and the adaptor complex elongin B/C to form CRL5 E3 ligases. The difference in the composition of the complex suggests that CUL5 works on different substrates compared with other family members (*61*). Our results provided in vivo evidence showing that *Cul5* deficiency triggered growth of breast cancers. Furthermore, we demonstrated that *Cul5* deficiency promoted tumorigenesis via microenvironmental changes, and increased CREB1 initiated the aggregation of monocytes and P-MDSCs to suppress the activity of T cells.

CREB1 is constitutively phosphorylated and overexpressed in various human cancers (*35*) and functions as an oncogene, with roles in tumorigenesis and activation in TNBC (*62*). In this study, we found that CREB1, which acts downstream of the MAPK pathway, was a main downstream of CUL5. This result could explain the exact mechanism through which CUL5 contributes to the MAPK pathway and provides clues for drug therapy in breast cancer treatment. CREB1 overexpression has been observed in esophageal cancer (*38*), and as a transcription factor, CREB1 is known to interact with the *TGFβ2* promoter to inhibit the transcription and expression of *TGF*β2, leading to a decrease in secreted CCL2 and blocking the extracellular signal–regulated kinase

pathway to inhibit cancer invasion. Our findings demonstrated similar downstream effects for CREB1 and showed that CREB1 inhibitors could be used in *Cul5*-deficient cells to inhibit tumor growth.

As an important member of the E3 ligase Cullin family, CUL5 has been reported to have several substrates, such as phosphorylated Cas, focal adhesions, Disabled-1, differential display and activation by p53, β-transducin repeat–containing protein, and DEPTOR (*52*). Together with CREB1, in our study, CUL5 has many downstream factors in different pathways. However, the roles of CUL5 in cell process are still not completely clear, and the mechanisms through which CUL5 selects its downstream factors in various biological processes have not been identified. Therefore, it may be important to elucidate the entire mechanical landscape of global protein metabolism. Further studies are needed to identify the mechanisms upstream of CUL5 in normal biological processes and evaluate the effects of CUL5 loss in patients with cancer. In summary, our findings established an effective approach to identify tumor suppressors in breast cancer, demonstrated the mechanisms of tumorigenesis under *Cul5*-deficient conditions, revealed the effects of TME changes on tumor growth, and provided insights into potential therapeutic strategies for breast cancer treatment.

MATERIALS AND METHODS

Animals

We used the following mouse strains in this study: (i) *Brca1* mammary gland–specific knockout mice mediated by the Cre-loxP approach (*Brca1*$^{Flox11/Flox11}$;*MMTV-Cre*) (*19*); (ii) *Brca1*$^{Flox11/Flox11}$;*MMTV-Cre* mice carrying the *Cul5* mutation generated by SB transposon insertion, as described previously (*16*); and (iii) *mT/mG* mice carrying a double-fluorescent reporter expressing membrane-targeted tandem dimer Tomato (mT) before CRE-mediated excision and membrane-targeted green fluorescent protein (mG) after excision (*63*). Because many transgenic strains were involved, the mice in this study had a mixed genetic background, including Black Swiss, FVB, and 129SVEV at roughly a 1:2:1 ratio. Only female mice were used for tumorigenesis, and tumor initiation and progression were monitored twice per week. All mouse experiments were approved by the ethical guidelines of the University of Macau (approval no. UMAEC-050-2015).

Plasmid construction

The primer sequence information is listed as follows. LentiCRISPRv2 (Addgene #52961), lentiCRISPRv2 blast (Addgene #98293), and lentiCRISPRv2 (Addgene #98291) were obtained from Addgene. We digested the plasmids with the restriction enzyme Esp 3I (BsmB I; New England Biolabs) and ligated the plasmids using the annealed sgRNA paired DNA sequences, as previously described (*64*). pCW57-MCS1-2A-MCS2 (Addgene #71782) is an all-in-one doxycycline-inducible lentiviral vector for gene expression. We integrated human *Cul5* cDNA from the plasmid pcDNA5/FRT-Flag-CUL5 (Addgene #31984) into pCW57-MCS1-2A-MCS2 and added a 3× Flag sequence on the 5′ terminal (Flag sequence: CGCGTATGGACTACAAAGACCATGACGGTGATTATAAAGATCATGATATCGATTACAAGGATGACGATGACAAGA). pcDNA3-myc-CUL5 (Addgene #19895) and pcDNA5/FRT-Flag-CUL5 (Addgene #31984) were purchased from Addgene.

Cell culture

Brca1-MT G600 (*Brca1*$^{\Delta 11/\Delta 11}$;*p53*$^{-/-}$) and *Brca1*-WT B447 (*Brca1*$^{+/+}$;*p53*$^{-/-}$) were derived from mammary epithelial cells of *Brca1*$^{\Delta 11/\Delta 11}$;*p53*$^{+/-}$ and *Brca1*$^{+/+}$;*p53*$^{+/-}$ mice, respectively, and were malignantly transformed spontaneously after loss of the WT allele of *p53* during culture condition (*11*). MEFs, MDA-MB-231, G600, B477, and human embryonic kidney (HEK) 293T cells were cultured in Dulbecco's modified Eagle's medium (DMEM; Gibco, USA). 4T1 cells, which is a TNBC line lacking *p53*, but WT for *Brca1* and *Brca2* (*65*) were cultured in 1640 (Gibco). The culture medium contained 10% fetal bovine serum (Gibco), penicillin (100 IU/ml; Gibco), and streptomycin (100 μg/ml; Gibco).

Generation of *Brca1*-deficient MEFs

Primary MEFs were obtained from mouse embryos at embryonic day E12.5. The cells were homozygous for loxP-flanked alleles of *Brca1* exon 11 in a background of *mT/mG* (*Brca1*$^{Flox11/Flox11}$;*mT/mG*). To knock out *Brca1* in MEFs, MEFs were infected with adenovirus containing CRE (1×10^{10} to 1×10^{11} plaque-forming units/ml) with a multiplicity of infection of greater than or equal to 10, and *Brca1*-mutant cells with green fluorescent protein–positive signals were isolated using FACS.

CRISPR-Cas9–mediated genome-wide screening

We generated *Brca1*-deficient MEFs for CRISPR-Cas9–mediated genome-wide screening as follows. First, we packaged the lentivirus with a loss-of-function mouse GeCKOv2 sgRNA library (Addgene, pooled library #1000000052), which included 123,666 sgRNAs targeting 20,611 genes, 4700 sgRNAs targeting 1175 microRNAs (miRNAs), and 1000 nontargeting sgRNAs as controls (*18*). Each gene had six sgRNAs targeting different nucleotide sites. Each miRNA had four sgRNAs targeting different nucleotide sites. The system contained a core vector with fused DNA sequences of Cas9 and sgRNA expression, vectors of △8.2, and VSVG to package the lentivirus. Lentiviruses were packaged in HEK293T cells and harvested 72 hours later. The lentiviruses were then concentrated to a titer of 10^8 U/ml, and *Brca1*-deficient MEFs were infected with a concentrated lentivirus packaging library or control. Last, DNA samples were isolated from cells at each generation, and tumors were prepared for Illumina second-generation sequencing.

Fat pad implantation

Female nude mice (4 to 6 weeks of age) were used for the experiments. Cells of different genotypes carrying mouse GeCKOv2 sgRNA were washed and suspended in phosphate-buffered saline (PBS) at a concentration of 10^7 cells/ml before being injected into the fourth pair of mammary glands with a maximum volume of 100 μl.

Second-generation sequencing

We generated DNA samples from cells or tumors and amplified the sgRNA region using the following primers: forward, GTAACTTGAAAGTATTTCGATTTCTTGGCTTTATATATCTTGTGGAAAGGACGAAACACC; reverse, ACTTTTCAAGTTGATAACGGACTAGCCTTATTTTAACTTGC TATTTCTAGCTCTAAAAC. Barcodes and indexes were added at the two ends of the amplified sgRNA, and all procedures were performed according to the protocol described by Joung *et al.* (*64*). The PCR products were quantified by DNA agarose gel electrophoresis on 2% (w/v) gels, and a successful

reaction generated a 260- to 270-bp product. The products were then purified using a QIAquick PCR purification kit (Qiagen, Valencia, CA, USA). We used an Agilent RNA 6000 NanoKit (Agilent, Palo Alto, USA) to confirm the purity, concentration, and exact size of the purified PCR products. We then sent the samples for Illumina second-generation sequencing.

CyTOF analysis

Separate cohorts of mouse tumor samples were analyzed using CyTOF. Tumors were excised and digested into single cells. Cells were washed with prewarmed serum-free medium and resuspended at 2×10^7 cells/ml in prewarmed serum-free medium, treated with 10 mM cisplatin for 5 min at room temperature, washed, incubated with antibody cocktails for 30 min at room temperature, and lastly fixed with Maxpar cell staining buffer (Fluidigm, USA). The fixed samples were sent for CyTOF analysis using Helios D16-0917 (Fluidigm, USA). The immune cells were distinguished using CD45 as a marker and divided into immune subtypes based on the express of different immune markers. Flow cytometry standard (FCS) files were manually gated in FlowJo (v10.0.7.2, BD). Single and living cells were filtered into FCS files. The data were normalized using bead-based normalization software [R package, cytofWorkflow_1.12.1 (*66*)]. Cluster analysis was performed using the R package (cytofWorkflow_1.12.1, HDCytoData_1.8.0, flowCore_2.0.1, and diffcyt_1.8.8).

Western blotting

Tissues were harvested, cut into small pieces, digested with radioimmunoprecipitation assay buffer (catalog no. 20-188; Millipore, USA) with phenylmethylsulfonyl fluoride (PMSF; 1 mM) and protease inhibitor cocktail (Roche, Swiss), and quantified using a BCA Protein Assay Kit (catalog no. 23225; Thermo Fisher Scientific, MA, USA). Protein lysates were denatured using 5× loading buffer solution [250 mM tris-HCl (pH 6.8), 30% (v/v) glycerol, 10% SDS, 0.05% (w/v) bromophenol blue, and 10 mM dithiothreitol (DTT) with 25% 2-mercaptoethanol] and incubated at 95°C for 10 min. Protein lysates were then electrophoresed on 8 to 12% SDS-polyacrylamide gels and transferred to polyvinylidene difluoride membranes (Millipore). The SDS running buffer and transfer buffer were obtained from Bio-Rad Laboratories (Hercules, CA, USA). The membranes were blocked in 3% bovine serum albumin with tris buffered saline with Tween 20(TBS-T) buffer [20 mM tris, 150 mM NaCl, and 0.1% Tween 20 (pH 7.4 to 7.6)] for 1 hour at room temperature and then incubated overnight with primary antibodies, including anti-CUL5 (1:1000; catalog no. ABN289; Millipore), anti-CREB1 (1:1000; catalog no. 4820 or 9191; Cell Signaling Technology, Danvers, MA), anti-CDC2L5 (1:200; catalog no. sc-81837; Santa Cruz Biotechnology, Santa Cruz, CA, USA), and anti–β-actin (1:5000; catalog no. A2228; Sigma-Aldrich, St. Louis, MO, USA). Membranes were washed three times with TBS-T buffer and incubated for 1 hour with a horseradish peroxidase–conjugated secondary antibody (1:5000; Cell Signaling Technology). Membranes were washed with TBS-T buffer and developed using enhanced chemiluminescence reagent (catalog no. WBULS0500; Millipore) with a digital imaging system (Bio-Rad Laboratories).

Immunoprecipitation

HEK293T cells were transfected with overexpression plasmids (10 μg per 10-cm dish) for 48 hours, washed, harvested in cold PBS, and lysed with Immunoprecipitation (IP) buffer (1-ml buffer/1×10^7 cells) supplemented with 1 mM PMSF and protease inhibitor cocktail (*67*) for 1 hour. Proteins in the obtained lysates were then quantified using a BCA Protein Assay Kit (catalog no. 23225; Thermo Fisher Scientific). The soluble components were separated by centrifugation at 12,000 rpm for 15 min. Next, 1 μg of specific antibody (1 to 2 μg of antibody/1 mg of protein) was added to the soluble fraction for immunoprecipitation, and samples were rotated for 1 hour at 4°C. Forty microliters of a 50% slurry of protein A/G-beads (catalog no. sc2003; Santa Cruz Biotechnology) was washed with IP buffer three times and incubated with soluble proteins overnight at 4°C. Immunoprecipitates were washed with PBS three times, and the immunoprecipitated proteins were denatured in 5× loading buffer solution [250 mM tris-HCl (pH 6.8), 30% (v/v) glycerol, 10% SDS, 0.05% (w/v) bromophenol blue, and 10 mM DTT with 25% 2-mercaptoethanol] at 95°C for 10 min. Then, the samples were detected by Western blotting.

Proteomic assay

We harvested cells without trypsin to avoid digesting the extracellular domains of the proteins on the cell surface. Cells were then washed with cold tris-buffered sucrose solution [250 mM sucrose and 10 mM tris-HCl (pH 7.0)] at 4°C, transferred (3.5×10^6 cells) to new tubes, and washed with PBS. Proteins were extracted using 500 μl of extraction buffer [0.02 M tris/HCl (pH 6.8), 2% SDS, and 0.1 M DTT; without protein inhibitors], resuspended, sonicated, and incubated at 56°C for 30 min. The supernatants were obtained after microcentrifugation at 14,000*g* for 5 min. Protein concentrations were then measured using Bio-Rad RC-DC protein assays with the concentration adjusted between 0.12 and 0.4 mg/ml. Protein samples were placed in a refrigerator at −80°C for further proteomic analysis.

Quantitative RT-PCR

RNA was extracted using TRIzol (catalog no. 15596026; Thermo Fisher Scientific) according to the manufacturer's protocols. cDNA was generated using a Qiagen OneStep RT-PCR kit (catalog no. 210212; Qiagen), and quantitative RT-PCR was performed using FastStart SYBR Green Master Mix (catalog no. 04913850001; Roche, IN, USA); the primer information is declared in table S3.

Immunofluorescence and IHC staining

Tissues were fixed in 10% formalin, embedded, and sectioned. The samples were fully deparaffinized in 100% xylene and rehydrated in ethanol at gradually lower concentrations. The slices were then soaked in citrate buffer (pH 6.0) and boiled in Retriever (Electron Microscopy Sciences, PA, USA) for antigen retrieval using standard procedures. For immunohistochemical (IHC) staining, the slices were stained with primary antibodies, followed by signal detection using a Signal Stain DAB Substrate Kit (Cell Signaling Technology, MA, USA). For immunofluorescence, the tissue samples or cells were fixed with 4% paraformaldehyde at room temperature and stained with primary antibodies, as described above. The general staining procedure was based on the standard protocols. Images were acquired using a BX53 microscope (Olympus, Japan).

Single-cell RNA sequencing

Tumors were cut into small pieces and washed with PBS for several times. The small tumor pieces were digested into single cells with digestion buffer A (*68*) for 60 to 90 min and incubated at 37°C. The cells were resuspended in DMEM, and each cell was picked one by one using a mouth pipette and transferred them into cold scRNA-seq lysis buffer on the ice; we picked about 100 cells in each group. Cells were extracted and sequenced using the previously described methods (*69*).

Statistical analysis

Data are presented as means ± SEs of the means. All data for paired comparisons were analyzed using Student's *t* tests, and results with *P* values less than 0.05 were considered statistically significant. All statistical evaluations were performed using GraphPad Prism software (version 6.0).

Supplementary Materials

This PDF file includes:
Figs. S1 to S8

Other Supplementary Material for this manuscript includes the following:
Tables S1 to S3

View/request a protocol for this paper from *Bio-protocol*.

REFERENCE AND NOTES

1. F. J. Sánchez-Rivera, T. Jacks, Applications of the CRISPR-Cas9 system in cancer biology. *Nat. Rev. Cancer* **15**, 387–393 (2015).
2. M. R. Stratton, P. J. Campbell, P. A. Futreal, The cancer genome. *Nature* **458**, 719–724 (2009).
3. X. Liu, E. Krawczyk, F. A. Suprynowicz, N. Palechor-Ceron, H. Yuan, A. Dakic, V. Simic, Y.-L. Zheng, P. Sripadhan, C. Chen, J. Lu, T. W. Hou, S. Choudhury, B. Kallakury, D. G. Tang, T. Darling, R. Thangapazham, O. Timofeeva, A. Dritschilo, S. H. Randell, C. Albanese, S. Agarwal, R. Schlegel, Conditional reprogramming and long-term expansion of normal and tumor cells from human biospecimens. *Nat. Protoc.* **12**, 439–451 (2017).
4. L. Cao, S. Kim, C. Xiao, R. H. Wang, X. Coumoul, X. Wang, W. M. Li, X. L. Xu, J. A. De Soto, H. Takai, S. Mai, S. J. Elledge, N. Motoyama, C.-X. Deng, ATM-Chk2-p53 activation prevents tumorigenesis at an expense of organ homeostasis upon Brca1 deficiency. *EMBO J.* **25**, 2167–2177 (2006).
5. J. M. Hall, M. K. Lee, B. Newman, J. E. Morrow, L. A. Anderson, B. Huey, M. C. King, Linkage of early-onset familial breast cancer to chromosome 17q21. *Science* **250**, 1684–1689 (1990).
6. Q. Wang, H. Zhang, S. Guerrette, J. Chen, A. Mazurek, T. Wilson, A. Slupianek, T. Skorski, R. Fishel, M. I. Greene, Adenosine nucleotide modulates the physical interaction between hMSH2 and BRCA1. *Oncogene* **20**, 4640–4649 (2001).
7. C. Engel, C. Fischer, S. Zachariae, K. Bucksch, K. Rhiem, J. Giesecke, N. Herold, B. Wappenschmidt, V. Hübbel, M. Maringa, S. Reichstein-Gnielinski, E. Hahnen, C. R. Bartram, N. Dikow, S. Schott, D. Speiser, D. Horn, E. M. Fallenberg, M. Kiechle, A. S. Quante, A.-S. Vesper, T. Fehm, C. Mundhenke, N. Arnold, E. Leinert, W. Just, U. Siebers-Renelt, S. Weigel, A. Gehrig, A. Wöckel, B. Schlegelberger, S. Pertschy, K. Kast, P. Wimberger, S. Briest, M. Loeffler, U. Bick, R. K. Schmutzler; German Consortium for Hereditary Breast, Ovarian Cancer (GC-HBOC), Breast cancer risk in *BRCA1/2* mutation carriers and noncarriers under prospective intensified surveillance. *Int. J. Cancer* **146**, 999–1009 (2020).
8. L. Hilakivi-Clarke, Estrogens, BRCA1, and breast cancer. *Cancer Res.* **60**, 4993–5001 (2000).
9. S. G. Brodie, X. Xu, W. Qiao, W. M. Li, L. Cao, C. X. Deng, Multiple genetic changes are associated with mammary tumorigenesis in Brca1 conditional knockout mice. *Oncogene* **20**, 7514–7523 (2001).
10. P. Bouwman, J. Jonkers, Mouse models for BRCA1 associated tumorigenesis: From fundamental insights to preclinical utility. *Cell Cycle* **7**, 2647–2653 (2008).
11. X. Xu, W. Qiao, S. P. Linke, L. Cao, W.-M. Li, P. A. Furth, C. C. Harris, C.-X. Deng, Genetic interactions between tumor suppressors Brca1 and p53 in apoptosis, cell cycle and tumorigenesis. *Nat. Genet.* **28**, 266–271 (2001).
12. L. Cao, W. Li, S. Kim, S. G. Brodie, C.-X. Deng, Senescence, aging, and malignant transformation mediated by p53 in mice lacking the Brca1 full-length isoform. *Genes Dev.* **17**, 201–213 (2003).
13. L. Cao, X. Xu, S. F. Bunting, J. Liu, R.-H. Wang, L. L. Cao, J. J. Wu, T.-N. Peng, J. Chen, A. Nussenzweig, C.-X. Deng, T. Finkel, A selective requirement for 53BP1 in the biological response to genomic instability induced by Brca1 deficiency. *Mol. Cell* **35**, 534–541 (2009).
14. S. F. Bunting, E. Callén, N. Wong, H.-T. Chen, F. Polato, A. Gunn, A. Bothmer, N. Feldhahn, O. Fernandez-Capetillo, L. Cao, X. Xu, C.-X. Deng, T. Finkel, M. Nussenzweig, J. M. Stark, A. Nussenzweig, 53BP1 inhibits homologous recombination in Brca1-deficient cells by blocking resection of DNA breaks. *Cell* **141**, 243–254 (2010).
15. A. J. Dupuy, L. M. Rogers, J. Kim, K. Nannapaneni, T. K. Starr, P. Liu, D. A. Largaespada, T. E. Scheetz, N. A. Jenkins, N. G. Copeland, A modified *sleeping beauty* transposon system that can be used to model a wide variety of human cancers in mice. *Cancer Res.* **69**, 8150–8156 (2009).
16. K. Miao, J. H. Lei, M. V. Valecha, A. Zhang, J. Xu, L. Wang, X. Lyu, S. Chen, Z. Miao, X. Zhang, S. M. Su, F. Shao, B. K. Rajendran, J. Bao, J. Zeng, H. Sun, P. Chen, K. Tan, Q. Chen, K. H. Wong, X. Xu, C.-X. Deng, NOTCH1 activation compensates BRCA1 deficiency and promotes triple-negative breast cancer formation. *Nat. Commun.* **11**, 3256 (2020).
17. X. Xu, Z. Weaver, S. P. Linke, C. Li, J. Gotay, X. W. Wang, C. C. Harris, T. Ried, C.-X. Deng, Centrosome amplification and a defective G2-M cell cycle checkpoint induce genetic instability in BRCA1 exon 11 isoform-deficient cells. *Mol. Cell* **3**, 389–395 (1999).
18. N. E. Sanjana, O. Shalem, F. Zhang, Improved vectors and genome-wide libraries for CRISPR screening. *Nat. Methods* **11**, 783–784 (2014).
19. X. Xu, K.-U. Wagner, D. Larson, Z. Weaver, C. Li, T. Ried, L. Hennighausen, A. Wynshaw-Boris, C.-X. Deng, Conditional mutation of *Brca1* in mammary epithelial cells results in blunted ductal morphogenesis and tumour formation. *Nat. Genet.* **22**, 37–43 (1999).
20. N. H. Chehab, A. Malikzay, M. Appel, T. D. Halazonetis, Chk2/hCds1 functions as a DNA damage checkpoint in G_1 by stabilizing p53. *Genes Dev.* **14**, 278–288 (2000).
21. R. L. Kurzhals, S. W. Titen, H. B. Xie, K. G. Golic, Chk2 and p53 are haploinsufficient with dependent and independent functions to eliminate cells after telomere loss. *PLOS Genet.* **7**, e1002103 (2011).
22. H. Meijers-Heijboer, A. van den Ouweland, J. Klijn, M. Wasielewski, A. de Snoo, R. Oldenburg, A. Hollestelle, M. Houben, E. Crepin, M. van Veghel-Plandsoen, F. Elstrodt, C. van Duijn, C. Bartels, C. Meijers, M. Schutte, L. M. Guffog, D. Thompson, D. Easton, N. Sodha, S. Seal, R. Barfoot, J. Mangion, J. Chang-Claude, D. Eccles, R. Eeles, D. G. Evans, R. Houlston, V. Murday, S. Narod, T. Peretz, J. Peto, C. Phelan, H. X. Zhang, C. Szabo, P. Devilee, D. Goldgar, P. A. Futreal, K. L. Nathanson, B. Weber, N. Rahman, M. R. Stratton; CHEK2-Breast Cancer Consortium, Low-penetrance susceptibility to breast cancer due to *CHEK2** 1100delC in noncarriers of *BRCA1* or *BRCA2* mutations. *Nat. Genet.* **31**, 55–59 (2002).
23. X. Xu, E. Chen, L. Mo, L. Zhang, F. Shao, K. Miao, J. Liu, S. M. Su, M. Valecha, U. I. Chan, H. Zheng, M. Chen, W. Chen, Q. Chen, H. Fu, M. I. Aladjem, Y. He, C.-X. Deng, BRCA1 represses DNA replication initiation through antagonizing estrogen signaling and maintains genome stability in parallel with WEE1–MCM2 signaling during pregnancy. *Hum. Mol. Genet.* **28**, 842–857 (2019).
24. J. C. Lal, M. G. Townsend, A. K. Mehta, M. Oliwa, E. Miller, A. Sotayo, E. Cheney, E. A. Mittendorf, A. Letai, J. L. Guerriero, Comparing syngeneic and autochthonous models of breast cancer to identify tumor immune components that correlate with response to immunotherapy in breast cancer. *Breast Cancer Res.* **23**, 83 (2021).
25. F. Mollinedo, Neutrophil degranulation, plasticity, and cancer metastasis. *Trends Immunol.* **40**, 228–242 (2019).
26. S. Cane, S. Ugel, R. Trovato, I. Marigo, F. De Sanctis, S. Sartoris, V. Bronte, The endless saga of monocyte diversity. *Front. Immunol.* **10**, 1786 (2019).
27. Q. Hao, J. V. Vadgama, P. Wang, CCL2/CCR2 signaling in cancer pathogenesis. *Cell Commun. Signal* **18**, 82 (2020).
28. S. Hai-Rim, A comment on 'global activity of cancer registries and cancer control and cancer incidence statistics in Korea'. *J Prev Med Public Health* **41**, 208–209; author reply 209–211 (2008).
29. J.-E. Alard, A. Ortega-Gomez, K. Wichapong, D. Bongiovanni, M. Horckmans, R. T. Megens, G. Leoni, B. Ferraro, J. Rossaint, N. Paulin, J. Ng, H. Ippel, D. Suylen, R. Hinkel, X. Blanchet, F. Gaillard, M. D'Amico, P. von Hundelshausen, A. Zarbock, C. Scheiermann, T. M. Hackeng, S. Steffens, C. Kupatt, G. A. Nicolaes, C. Weber, O. Soehnlein, Recruitment of classical monocytes can be inhibited by disturbing heteromers of neutrophil HNP1 and platelet CCL5. *Sci. Transl. Med.* **7**, 317ra196 (2015).
30. Q. Zhao, T. Kim, J. Pang, W. Sun, X. Yang, J. Wang, Y. Song, H. Zhang, H. Sun, V. Rangan, S. Deshpande, H. Tang, M. E. Cvijic, R. Westhouse, T. Olah, J. Xie, M. Struthers, L. Salter-Cid, A novel function of CXCL10 in mediating monocyte production of proinflammatory cytokines. *J. Leukoc. Biol.* **102**, 1271–1280 (2017).
31. A. Giladi, L. K. Wagner, H. Li, D. Dörr, C. Medaglia, F. Paul, A. Shemer, S. Jung, S. Yona, M. Mack, A. Leutz, I. Amit, A. Mildner, *Cxcl10*$^+$ monocytes define a pathogenic subset in the

central nervous system during autoimmune neuroinflammation. *Nat. Immunol.* **21**, 525–534 (2020).
32. M. Metzemaekers, A. Mortier, A. Vacchini, D. Boff, K. Yu, R. Janssens, F. M. Farina, S. Milanesi, N. Berghmans, N. Pörtner, J. Van Damme, M. Allegretti, M. M. Teixeira, M. Locati, E. M. Borroni, F. A. Amaral, P. Proost, Endogenous modification of the chemoattractant CXCL5 alters receptor usage and enhances its activity toward neutrophils and monocytes. *Sci. Signal.* **14**, eaax3053 (2021).
33. G. Balamayooran, S. Batra, S. Cai, J. Mei, G. S. Worthen, A. L. Penn, S. Jeyaseelan, Role of CXCL5 in leukocyte recruitment to the lungs during secondhand smoke exposure. *Am. J. Respir. Cell Mol. Biol.* **47**, 104–111 (2012).
34. A. Y. Wen, K. M. Sakamoto, L. S. Miller, The role of the transcription factor CREB in immune function. *J. Immunol.* **185**, 6413–6419 (2010).
35. K. M. Sakamoto, D. A. Frank, CREB in the pathophysiology of cancer: Implications for targeting transcription factors for cancer therapy. *Clin. Cancer Res.* **15**, 2583–2587 (2009).
36. F. Okumura, A. Joo-Okumura, K. Nakatsukasa, T. Kamura, The role of cullin 5-containing ubiquitin ligases. *Cell Div.* **11**, 1 (2016).
37. F. Shao, X. Lyu, K. Miao, L. Xie, H. Wang, H. Xiao, J. Li, Q. Chen, R. Ding, P. Chen, F. Xing, X. Zhang, G.-H. Luo, W. Zhu, G. Cheng, N. W. Lon, S. E. Martin, G. Wang, G. Chen, Y. Dai, C.-X. Deng, Enhanced protein damage clearance induces broad drug resistance in multitype of cancers revealed by an evolution drug-resistant model and genome-wide siRNA screening. *Adv. Sci. (Weinh)* **7**, 2001914, 2001914 (2020).
38. W. W. Xu, Z.-H. Huang, L. Liao, Q.-H. Zhang, J.-Q. Li, C.-C. Zheng, Y. He, T.-T. Luo, Y. Wang, H.-F. Hu, Q. Zuo, W.-Y. Chen, Q.-S. Yang, J.-F. Zhao, Y. R. Qin, L.-Y. Xu, E.-M. Li, H.-X. Liao, B. Li, Q.-Y. He, Direct targeting of CREB1 with imperatorin Inhibits TGFβ2-ERK signaling to suppress esophageal cancer metastasis. *Adv Sci (Weinh)* **7**,2000925(2020).
39. V. Ollivier, G. C. Parry, R. R. Cobb, D. de Prost, N. Mackman, Elevated cyclic AMP inhibits NF-κB-mediated transcription in human monocytic cells and endothelial cells. *J. Biol. Chem.* **271**, 20828–20835 (1996).
40. G. C. Parry, N. Mackman, Role of cyclic AMP response element-binding protein in cyclic AMP inhibition of NF-kappaB-mediated transcription. *J. Immunol.* **159**, 5450–5456 (1997).
41. J. M. Park, F. R. Greten, A. Wong, R. J. Westrick, J. S. Arthur, K. Otsu, A. Hoffmann, M. Montminy, M. Karin, Signaling pathways and genes that inhibit pathogen-induced macrophage apoptosis—CREB and NF-κB as key regulators. *Immunity* **23**, 319–329 (2005).
42. T. Kitamura, B.-Z. Qian, J. W. Pollard, Immune cell promotion of metastasis. *Nat. Rev. Immunol.* **15**, 73–86 (2015).
43. S. K. Biswas, A. Mantovani, Macrophage plasticity and interaction with lymphocyte subsets: Cancer as a paradigm. *Nat. Immunol.* **11**, 889–896 (2010).
44. Y. Chen, J. Kim, S. Yang, H. Wang, C.-J. Wu, H. Sugimoto, V. S. LeBleu, R. Kalluri, Type I collagen deletion in αSMA$^+$ myofibroblasts augments immune suppression and accelerates progression of pancreatic cancer. *Cancer Cell* **39**, 548–565.e6 (2021).
45. B.-Z. Qian, J. Li, H. Zhang, T. Kitamura, J. Zhang, L. R. Campion, E. A. Kaiser, L. A. Snyder, J. W. Pollard, CCL2 recruits inflammatory monocytes to facilitate breast-tumour metastasis. *Nature* **475**, 222–225 (2011).
46. S. Y. Lim, A. E. Yuzhalin, A. N. Gordon-Weeks, R. J. Muschel, Targeting the CCL2-CCR2 signaling axis in cancer metastasis. *Oncotarget* **7**, 28697–28710 (2016).
47. D. I. Gabrilovich, S. Ostrand-Rosenberg, V. Bronte, Coordinated regulation of myeloid cells by tumours. *Nat. Rev. Immunol.* **12**, 253–268 (2012).
48. N. V. Serbina, E. G. Pamer, Monocyte emigration from bone marrow during bacterial infection requires signals mediated by chemokine receptor CCR2. *Nat. Immunol.* **7**, 311–317 (2006).
49. C. V. Jakubzick, G. J. Randolph, P. M. Henson, Monocyte differentiation and antigen-presenting functions. *Nat. Rev. Immunol.* **17**, 349–362 (2017).
50. Z. Shen, S. Kuang, M. Zhang, X. Huang, J. Chen, M. Guan, W. Qin, H. H. K. Xu, Z. Lin, Inhibition of CCL2 by bindarit alleviates diabetes-associated periodontitis by suppressing inflammatory monocyte infiltration and altering macrophage properties. *Cell. Mol. Immunol.* **18**, 2224–2235 (2020).
51. L. Jia, Y. Sun, SCF E3 ubiquitin ligases as anticancer targets. *Curr. Cancer Drug Targets* **11**, 347–356 (2011).
52. F. Gao, Y. Fan, B. Zhou, W. Guo, X. Jiang, J. Shi, C. Ren, The functions and properties of cullin-5, a potential therapeutic target for cancers. *Am. J. Transl. Res.* **12**, 618–632 (2020).
53. G. Zhao, L. Gong, D. Su, Y. Jin, C. Guo, M. Yue, S. Yao, Z. Qin, Y. Ye, Y. Tang, Q. Wu, J. Zhang, B. Cui, Q. Ding, H. Huang, L. Hu, Y. Chen, P. Zhang, G. Hu, L. Chen, K.-K. Wong, D. Gao, H. Ji, Cullin5 deficiency promotes small-cell lung cancer metastasis by stabilizing integrin β1. *J. Clin. Invest.* **129**, 972–987 (2019).
54. M. A. Tapia-Laliena, N. Korzeniewski, S. Peña-Llopis, C. Scholl, S. Fröhling, M. Hohenfellner, A. Duensing, S. Duensing, Cullin 5 is a novel candidate tumor suppressor in renal cell carcinoma involved in the maintenance of genome stability. *Oncogenesis* **8**, 4 (2019).
55. J. G. Zhang, A. Farley, S. E. Nicholson, T. A. Willson, L. M. Zugaro, R. J. Simpson, R. L. Moritz, D. Cary, R. Richardson, G. Hausmann, B. T. Kile, S. B. Kent, W. S. Alexander, D. Metcalf, D. J. Hilton, N. A. Nicola, M. Baca, The conserved SOCS box motif in suppressors of cytokine signaling binds to elongins B and C and may couple bound proteins to proteasomal degradation. *Proc. Natl. Acad. Sci. U.S.A.* **96**, 2071–2076 (1999).
56. C. Van Dort, P. Zhao, K. Parmelee, B. Capps, A. Poel, L. Listenberger, J. Kossoris, B. Wasilevich, D. Murrey, P. Clare, M. Burnatowska-Hledin, VACM-1, a cul-5 gene, inhibits cellular growth by a mechanism that involves MAPK and p53 signaling pathways. *Am. J. Physiol. Cell Physiol.* **285**, C1386–C1396 (2003).
57. R. Lang, A.-L. Pauleau, E. Parganas, Y. Takahashi, J. Mages, J. N. Ihle, R. Rutschman, P. J. Murray, SOCS3 regulates the plasticity of gp130 signaling. *Nat. Immunol.* **4**, 546–550 (2003).
58. M. Antonioli, F. Albiero, F. Nazio, T. Vescovo, A. B. Perdomo, M. Corazzari, C. Marsella, P. Piselli, C. Gretzmeier, J. Dengjel, F. Cecconi, M. Piacentini, G. M. Fimia, AMBRA1 interplay with cullin E3 ubiquitin ligases regulates autophagy dynamics. *Dev. Cell* **31**, 734–746 (2014).
59. W. Li, C. Xiao, B. K. Vonderhaar, C.-X. Deng, A role of estrogen/ERα signaling in BRCA1-associated tissue-specific tumor formation. *Oncogene* **26**, 7204–7212 (2007).
60. F. E. Morreale, H. Walden, Types of ubiquitin ligases. *Cell* **165**, 248–248.e1 (2016).
61. Z. Chen, J. Sui, F. Zhang, C. Zhang, Cullin family proteins and tumorigenesis: Genetic association and molecular mechanisms. *J. Cancer* **6**, 233–242 (2015).
62. Y. Qin, W. Chen, G. Jiang, L. Zhou, X. Yang, H. Li, X. He, H.-L. Wang, Y.-B. Zhou, S. Huang, S. Liu, Interfering MSN-NONO complex-activated CREB signaling serves as a therapeutic strategy for triple-negative breast cancer. *Sci. Adv.* **6**, eaaw9960 (2020).
63. M. D. Muzumdar, B. Tasic, K. Miyamichi, L. Li, L. Luo, A global double-fluorescent Cre reporter mouse. *Genesis* **45**, 593–605 (2007).
64. J. Joung, S. Konermann, J. S. Gootenberg, O. O. Abudayyeh, R. J. Platt, M. D. Brigham, N. E. Sanjana, F. Zhang, Genome-scale CRISPR-Cas9 knockout and transcriptional activation screening. *Nat. Protoc.* **12**, 828–863 (2017).
65. B. Schrörs, S. Boegel, C. Albrecht, T. Bukur, V. Bukur, C. Holtsträter, C. Ritzel, K. Manninen, A. D. Tadmor, M. Vormehr, U. Sahin, M. Löwer, Multi-omics characterization of the 4T1 murine mammary gland tumor model. *Front. Oncol.* **10**, 1195 (2020).
66. M. Nowicka, C. Krieg, H. L. Crowell, L. M. Weber, F. J. Hartmann, S. Guglietta, B. Becher, M. P. Levesque, M. D. Robinson, CyTOF workflow: Differential discovery in high-throughput high-dimensional cytometry datasets. *F1000Res* **6**, 748 (2017).
67. F. Guénard, C. S. Pedneault, G. Ouellette, Y. Labrie, J. Simard; INHERIT, F. Durocher, Evaluation of the contribution of the three breast cancer susceptibility genes CHEK2, STK11, and PALB2 in non-BRCA1/2 French Canadian families with high risk of breast cancer. *Genet. Test Mol. Biomarkers* **14**, 515–526 (2010).
68. H. Sun, X. Xu, C.-X. Deng, Preparation of single epithelial cells suspension from mouse mammary glands. *Bio Protoc.* **10**, e3530 (2020).
69. S. Gao, L. Yan, R. Wang, J. Li, J. Yong, X. Zhou, Y. Wei, X. Wu, X. Wang, X. Fan, J. Yan, X. Zhi, Y. Gao, H. Guo, X. Jin, W. Wang, Y. Mao, F. Wang, L. Wen, W. Fu, H. Ge, J. Qiao, F. Tang, Tracing the temporal-spatial transcriptome landscapes of the human fetal digestive tract using single-cell RNA-sequencing. *Nat. Cell Biol.* **20**, 721–734 (2018).

Acknowledgments: We would like to thank H. Shen (Faculty of Health Sciences, University of Macau) and G. Lu (Department of Physiology and Yong Loo Lin School of Medicine, National University of Singapore, Singapore, Singapore) for the technical help during ubiquitination assay. We also thank D. Gao (State Key Laboratory of Cell Biology, Innovation Center for Cell Signaling Network, CAS Center for Excellence in Molecular Cell Science, Shanghai Institute of Biochemistry and Cell Biology, Chinese Academy of Sciences, University of Chinese Academy of Sciences, Shanghai, China) for the technical assistance. We thank the members of the C.-X.D. and X.X. laboratories for helpful advice and discussions. We are grateful for the support of the animal facility core of the Faculty of Health Sciences, University of Macau. **Funding:** This work was supported by Chair Professor Grant (CPG2022-00002-FHS) from University of Macau, Macau SAR, China; Multiyear research grant (MYRG2022-00181-FHS) from University of Macau, Macau SAR, China; Macao Science and Technology Development Fund (FDCT: 111/2017/A, 0011/2019/AKP, FDCT-0004-2021-AKP, 0048/2019/A1, 0112/2019/A2, 0065/2021/A, and 0034/2019/AGJ); and Natural Science Foundation of China: 82030094 and 81602587. **Author contributions:** S.C. conceived, performed, and analyzed experiments, prepared figures, and wrote the manuscript. K.M. provided mouse samples and data analysis in SB screening, helped with ES cell assay, and provided advice on in vitro and in vivo experiments. J.Z. helped with most bioinformatic analysis in both primary and revision procedure. S.G. provided 4T1 cells, cowrote the manuscript, and provided advice in TME part. X.L. provided bioinformatic analysis in IHC experiments. H.S., H.J.L., and L.W. provided antibodies, reagents of IHC, and FACS assay. H.S. and Q.C. provided advice in logic design. F.S. developed some previously unidentified data in the revision procedure, provided the drugs, and the treatment conditions for protein damage assay. S.G. provided help for the single-cell sequencing. C.-X.D. and X.X. conceived the study, supervised experiments and data analysis, and cowrote the manuscript. All authors read and approved the final manuscript. **Competing interests:** The authors declare that they have no

competing interests. **Data and materials availability:** All data needed to evaluate the conclusions in the paper are present in the paper and/or the Supplementary Materials.

Submitted 4 April 2022
Accepted 16 December 2022
Published 20 January 2023
10.1126/sciadv.abq1395